Research Activities

– Synchrotron Radiation Experiments –

Angle resolved photoemission spectroscopy of Kondo lattice $YbNi_3Ga_9$

A. Rousuli[a], T. Nagasaki[b], H. Sato[c], H. Anzai[d], E. F. Schwier[c], M. Zheng[a],
Y. Kojima[a], H. Iwasawa[c], K. Shimada[c], K. Mimura[d], S. Ohara[e],
H. Namatame[c] and M. Taniguchi[a,c]

[a]Graduate School of Science, Hiroshima University, Higashi-Hiroshima 739-8526, Japan
[b]Faculty of Science, Hiroshima University, Higashi-Hiroshima 739-8526, Japan
[c]Hiroshima Synchrotron Radiation Center, Hiroshima University, Higashi-Hiroshima 739-0046, Japan
[d]Graduate School of Engineering, Osaka Prefecture University, Sakai 599-8531, Japan
[e]Graduate School of Engineering, Nagoya Institute of Technology, Nagoya 466-8555, Japan

Keywords: Yb-compounds, 4f electrons, valence fluctuation

In the strongly correlated 4f-electron system, the hybridization of conduction and 4f electrons (c-f hybridization) produces the various physical properties such as heavy-fermion behavior, magnetic transitions, valence fluctuation and superconductivity. Recently, Ohara *et al.* has discovered new Yb-based Kondo lattice compounds $YbNi_3X_9$ (X=Al, Ga) [1]. $YbNi_3Al_9$ is a heavy-fermion antiferromagnet with the Néel temperature of T_N=3.4 K while $YbNi_3Ga_9$ a non-magnetic valence fluctuation compound [1]. We have investigated their electronic structure by means of hard x-ray photoemission spectroscopy (PES) at hν = 6 keV and revealed that the Yb valence is nearly 3 for $YbNi_3Al_9$, while around 2.5 for $YbNi_3Ga_9$, indicating the strong c-f hybridization [2]. In this study, we have carried out angle resolved PES (ARPES) on $YbNi_3Ga_9$ in order to clarify their band structures due to the strong c-f hybridization near the Fermi level (E_F) and also on the reference compound $LuNi_3Ga_9$ for comparison. The ARPES experiments were performed at undulator beamline BL-1 of Hiroshima Synchrotron Radiation Center (HSRC). The ARPES spectra were collected at hν = 50 eV and 12 K along the ΓM and ΓK direction of the surface Brillouin zone.

Figure 1 shows the ARPES intensity plots of $LuNi_3Ga_9$ along ΓM and ΓK directions taken with the p-polarized configuration. A vertical axis represents binding energy relative to E_F and a horizontal axis angle along each direction. Bright area corresponds to the energy dispersions. We notice three or four bands crossing E_F and forming hole pockets around the Γ point. An electron pocket observed around ±10 deg. along ΓM disappears along ΓK. The most intense band around 15 deg. along ΓK, which is not detected along ΓM, makes a small pocket around K point. Although obtained ARPES intensity plot of $YbNi_3Ga_9$ is blurred, the c-f hybridization gap is marginally detected.

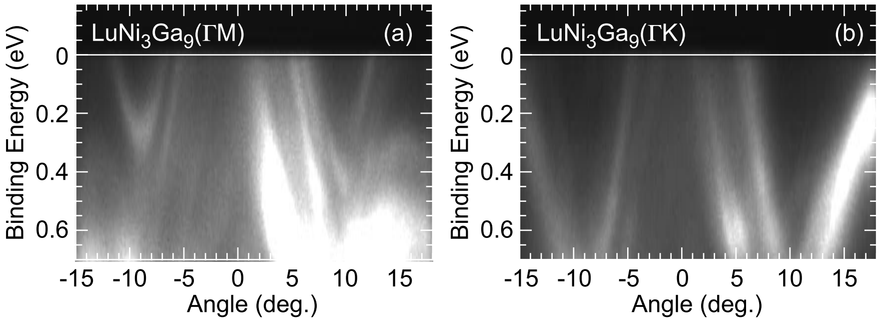

FIGURE 1. ARPES intensity plots of $LuNi_3Al_9$ along (a) ΓM and (b) ΓK directions measured at hν = 50 eV.

1. S. Ohara *et al.*, J. Phys.: Conf. Ser. **273**, 012048 (2011); T. Yamashita *et al.*, J. Phys. Soc. Jpn, **81**, 034705 (2012).
2. Y. Utsumi *et al.*, Phys. Rev. B **86**, 115114 (2012).

13-B-20, 14-A-9, 14-A-10 BL-1

The electronic structure of Monolayer $PtSe_2$

Wei Yao[1], Eryin Wang[1], Eike F. Schwier[3], Hideaki Iwasawa[3], Kenya Shimada[3], Masaki Taniguchi[3], Shuyun Zhou[1,2]

a. State Key Laboratory of Low-Dimensional Quantum Physics and Department of Physics, Tsinghua University, Beijing 100084, China
b. Collaborative Innovation Center of Quantum Matter, Beijing 100084, China
c. Hiroshima Synchrotron Radiation Center, Hiroshima University, Kagamiyama 2-313, Higashi-Hiroshima 739-0046, Japan

Keywords: $PtSe_2$, monolayer, transition-metal dichalcogenides

Two-dimensional layered materials such as transition-metal dichalcogenides (TMDs) recently have attracted research interests due to its novel physical properties [1-3]. First, the broken inversion symmetry in the crystal structure leads to large contrast between the two sets of “valley” in band structure and spin texture. Similar to spintronics, the concept of “valleytronics” is put forward for its potential application [3]. Second, the electronic structure of TMDs shows strong quantum confinement effect. By decreasing the sample thickness down to monolayer, various novel properties have been predicted and verified experimentally. For example, an indirect-to-direct bandgap transition from bulk to monolayer thin film has been reported for $MoSe_2$ [4]. However, so far research efforts on TMDs have focused only on a few materials such as MoS_2, $MoSe_2$, WS_2 and WSe_2. A large number of other members in TMDs family with various thickness remain unexplored due to the difficulty of sample growth. Here, we report a method for growing monolayer $PtSe_2$ -- a heretofore-unexplored member of the single-layer TMDs family – by direct selenization on Pt substrate. The $PtSe_2$ is verified by LEED and ARPES measurements. More importantly, ARPES measurements show monolayer $PtSe_2$ is a semiconductor with a sizable gap, which is very different from the semiconducting bulk $PtSe_2$. Such a gap may have potential applications, e.g. in photocatalysis.

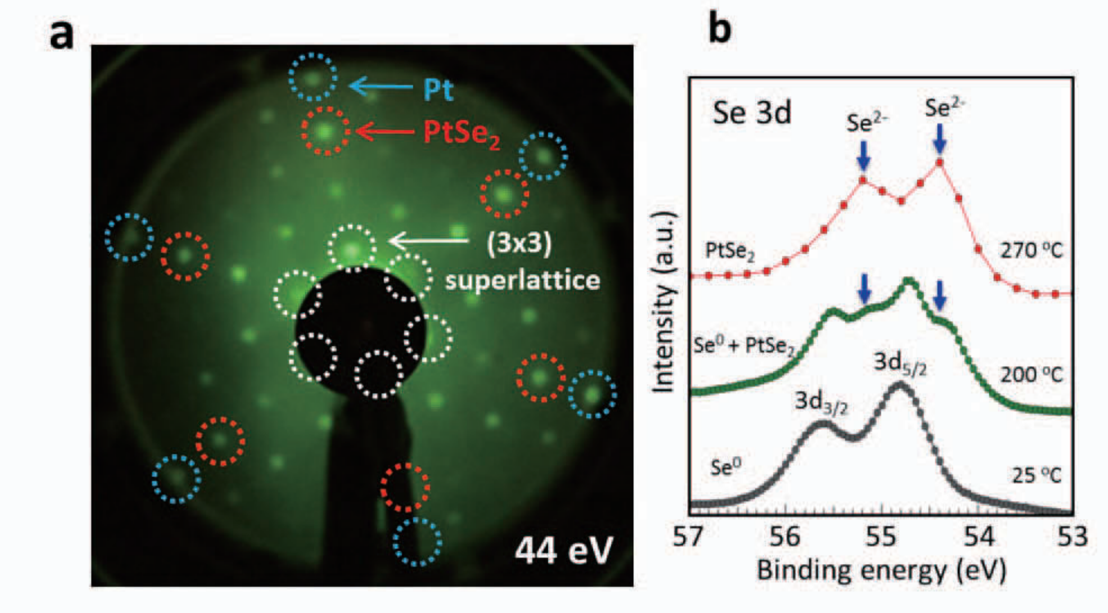

FIGURE. 1 (a) LEED pattern of as-grown monolayer PtSe$_2$. The spots indicated by blue, red and white circles are from Pt substrate, PtSe$_2$ and 3x3 superlattice respectively. (b) XPS data obtained during sample growth at 25 ℃, 200 ℃ and 270 ℃ respectively. From Ref. [7].

The monolayer PtSe$_2$ thin film is grown by a simple method – annealing Pt(111) substrate after depositing Se on the surface. The annealing temperature was slowly increased up to about 270 ℃. Figure 1(a) shows the LEED pattern after growth. By calculation, we identify that the spots indicated by red arrow are from PtSe$_2$. There are three orientations observed in LEED pattern, however only the one parallel to Pt(111) is dominant. The other spots indicated by white arrow in LEED pattern are from a 3x3 reconstruction due to mismatch between the lattice constants of PtSe$_2$ and Pt(111). The XPS measurement are used to monitor the growth process and shown in Fig 1(b). At room temperature, the Se 3d core level splits into two peaks. After annealing to 270 ℃, the two peaks evolve into the other two peaks at lower binding energy corresponding to Se^{2-} state. This result further confirms the formation of PtSe$_2$.

The electronic band structure of PtSe$_2$ thin film is investigated using angle-resolved photoemission spectroscopy. Figure 2 shows the ARPES data along the high symmetry direction. Figure 2(c) are the raw data and Figure 2(d) is the second derivative spectrum of the raw data to enhance visibility of the bands. Comparing with DFT calculation (Fig 3(c)), we find our data has best agreement to the band structure of monolayer PtSe$_2$, confirming that our sample has thickness of monolayer. In further calculation, the energy band of monolayer and bulk PtSe$_2$ have different structure: the monolayer one is semiconducting with a gap of 1.2 eV and the bulk one is semimetallic [5]. Such a transition in electronic structure [6] provides potential applications, for example, in the area of optoelectronics and photocatalysis.

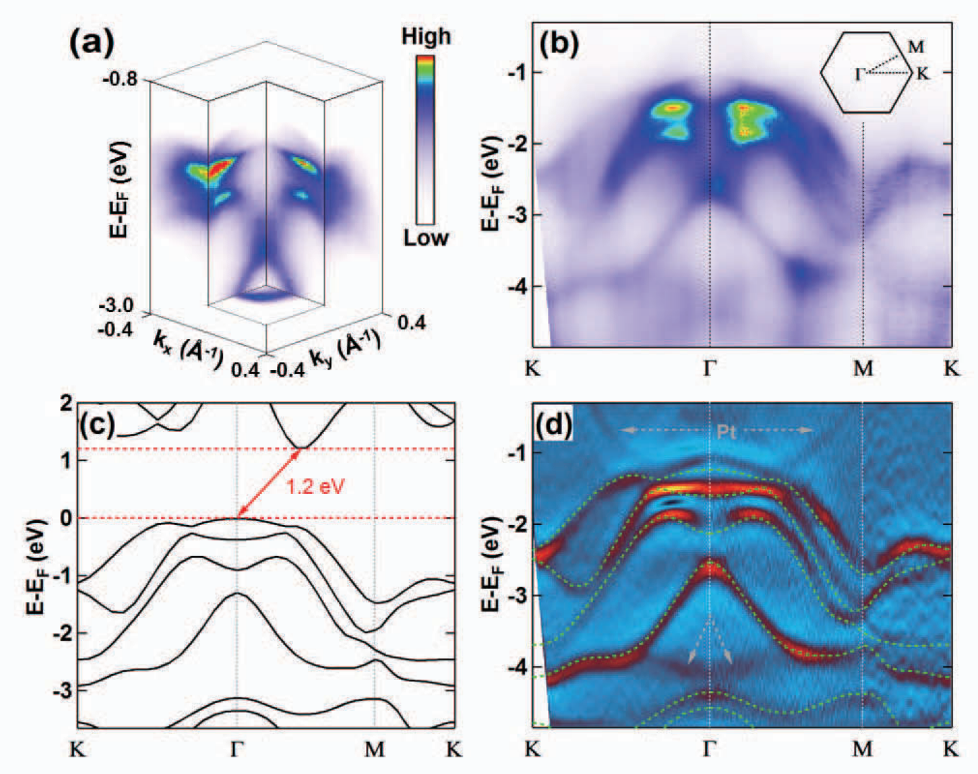

FIGURE. 2 (a) the overview of ARPES result. (b) measured ARPES data along K-Γ-M-K high symmetry direction. (c) the calculated band structure of monolayer $PtSe_2$ by DFT, showing an energy gap of 1.2 eV. (d) the second derivative spectrum of (b), which is superposed by the calculation result (green dashed lines) from (c).

In summary, we have successfully grown monolayer $PtSe_2$ thin film by direct annealing Pt substrate to 270 ℃ after depositing Se on it. LEED and XPS measurements confirm the formation of $PtSe_2$ with high crystalline quality. ARPES measurements reveal the band structure of monolayer $PtSe_2$ for the first time, showing its semiconducting behavior and suggesting the potential applications. This work has been published in Nano Lett. [7].

REFERENCE

[1] Q.H. Wang et al., Electronics and optoelectronics of two-dimensional transition metal dichalcogenides. Nat. Nano. 7, 699-712 (2012)

[2] M. Chhowalla et al., The chemistry of two-dimensional layered transition metal dichalcogenide nanosheets, Nat. Chem. 5, 263 (2013).

[3] X.D. Xu et al. Spin and pseudospins in layered transition metal dichalcogenides.Nat. Phys. 10, 343–350 (2014)

[4] Y.Zhang et al., Direct observation of the transition from indirect to direct bandgap in atomically thin epitaxial MoSe2, Nat. Nano. 9, 111-115 (2014)

[5] D. Dai et al., Trends in the structure and bonding in the layered platinum dioxide and dichalcogenides PtQ2 (Q=O, S, Se, Te), J. Solid State Chem. 173, 114 (2003).

[6] H.L. Zhuang and R.G. Hennig, compuetational search for single-layer transition-metal dichalcogenide photocatalysis, J. Phys. Chem. 117, 20440 (2013).

[7] Yeliang Wang$^+$, Linfei Li$^+$, Wei Yao$^+$, Shiru Song$^+$, J.T. Sun, Jinbo Pan, Xiao Ren, Chen Li, Eiji Okunishi, Yu-Qi Wang, Eryin Wang, Yan Shao, Y.Y. Zhang, Hai-tao Yang, Eike F. Schwier, Hideaki Iwasawa, Kenya Shimada, Masaki Taniguchi, Zhaohua Cheng, Shuyun Zhou*, Shixuan Du*, Stephen J. Pennycook, Sokrates T. Pantelides and Hong-Jun Gao*, “Monolayer PtSe$_2$, a new semiconducting transition-metal-dichalcogenide, epitaxially grown by direct selenization of Pt”, Nano Lett., in press (DOI: 10.1021/acs.nanolett.5b00964) (2015) http://pubs.acs.org/doi/abs/10.1021/acs.nanolett.5b00964

Angle-Resolved Photoemission Study of Heavy Fermion Compound EuNi$_2$P$_2$

H. Anzai[a], K. Ichiki[a], A. Hariki[a], R. Takeshita[a], H. Iwasawa[b], Eike F. Schwier[b], K. Shimada[b], H. Namatame[b], M. Taniguchi[b,c], A. Mitsuda[d], H. Wada[d], and K. Mimura[a,b]

[a] *Graduate School of Engineering, Osaka Prefecture University, Sakai 599-8531, Japan*
[b] *Hiroshima Synchrotron Radiation Center (HSRC), Hiroshima University, Higashi-Hiroshima 739-0046, Japan*
[c] *Graduate School of Science, Hiroshima University, Higashi-Hiroshima 739-8526, Japan*
[d] *Graduate School of Science, Kyushu University, Fukuoka 812-8581, Japan*

Keywords: *f*-electron, Electronic structure, angle-resolved photoemission spectroscopy.

Europium compounds are known to show a variety of magnetic and thermal properties due to existence of two components of Eu^{2+} and Eu^{3+} states [1]. In particular, EuNi$_2$P$_2$ has received much attention because it shows both mixed-valence and heavy-fermion behaviors. Indeed, the Mössbauer isomer-shift measurements show that EuNi$_2$P$_2$ is a mixed-valence compound, which varies its Eu mean valence between 2.25 at 300 K and 2.50 at zero temperature [2], and the coefficient of electronic specific heat is a large value of $\gamma \sim 100$ mJ/ (K^2·mol) [3]. It has been recently found that the single crystalline EuNi$_2$P$_2$ shows an anomalous thermal expansion and its scaling relation to the Eu mean valence [4]. The 4*f* electronic contribution to the thermal volume expansion, $(\Delta V/V)_{4f}$, decreases rapidly below 100 K and scales very well to temperature dependence of the Eu mean valence. This anomalous shrinkage of the $(\Delta V/V)_{4f}$ reflects the evolution of the heavy fermion state in EuNi$_2$P$_2$ with decreasing temperature and may be related to the hybridization between the Eu 4*f* states and conduction bands [4]. Hence, the electronic structure near the Fermi energy (E_F) provides important information for understanding of the mechanisms of the heavy fermion state in EuNi$_2$P$_2$.

Here, we report the angle-resolved photoemission spectroscopy (ARPES) measurements of the electronic structure of EuNi$_2$P$_2$, revealing that Ni 3d_{xy} and/or d_{yz} states are relevant to heavy-fermion behavior. The ARPES measurements were performed at BL-1 of Hiroshima Synchrotron Radiation Center, where two different polarization geometries of horizontal (*p* polarization) and vertical (*s* polarization) are achieved, as schematically shown in Fig. 1(b). All the data were taken with 70 eV photons in the *s* polarization geometry. The samples were cleaved *in situ* and kept under ultrahigh vacuum better than 5×10^{-11} Torr. Total energy resolution was set to 25 meV.

The electronic structure of EuNi$_2$P$_2$ taken with *s*-polarized photons is shown in Fig. 1. The band structures as indicated by the dashed curves in Fig. 1(c) are guides to the eyes. Three bands, α, β and γ, have been clearly identified, indicating their odd nature with respect to the mirror plane. Therefore, these bands are attributed to 3d_{xy} and/or d_{yz} orbitals. The α band crosses E_F and forms a hole pocket around X point, as shown in Fig. 1(a). We note that some certain bands may be missing in the measurements due to the matrix element effects and the energy resolution [5]. Further investigations for data taken with the *p*-polarized photon are in future work.

The temperature dependence of energy distribution curves (EDCs) is shown in Figs. 1(d) and 1(e). At the X point, two peaks corresponding to the β and γ bands are observed around $|\omega| \sim 1.7$ and 0.7 eV, respectively. Whereas the rising peak of the γ band is due to the thermal sharpening effect, the peak of the β band suddenly rises below 180 K. At the Γ point, a broad shoulder around $|\omega| \sim 1.2$ eV evolves into a sharp peak structure with decreasing temperatures. In order to reveal the relation between this anomalous evolution and heavy fermion state, we have quantified the intensity change of the β band from the temperature-dependent EDCs. The change between maximum and minimum intensities is normalized 100% after subtracting the linear background. As shown in Fig. 1(f), the change of the intensity both at Γ and X points starts around 150 K and tends to have no saturation at low temperatures. This temperature dependence is consistent with the overall feature of the 4*f* electronic contribution to the thermal volume expansion $(\Delta V/V)_{4f}$ [4].

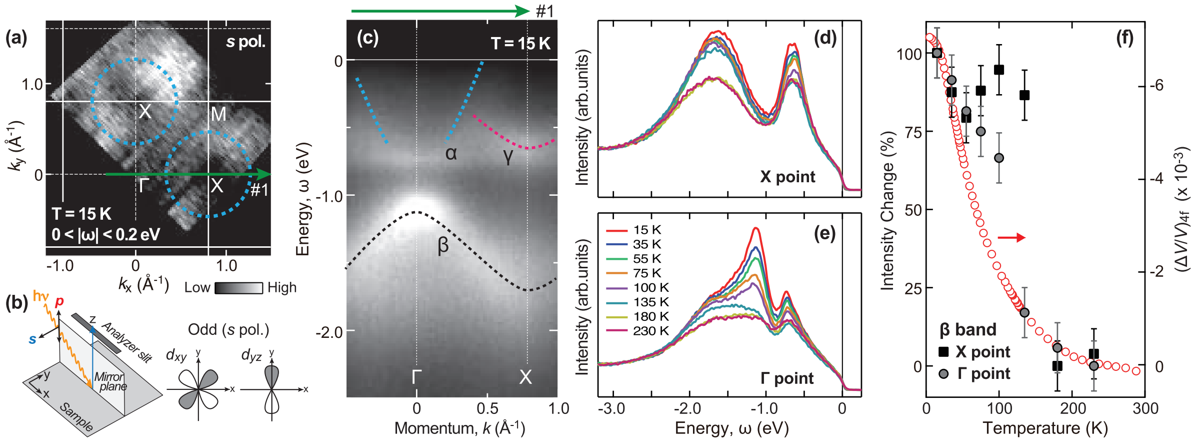

Figure 1. Electronic structure of $EuNi_2P_2$ taken with *s* polarized photons. (**a**) Photoemission intensity map as functions of k_x and k_y integrated over $0 < |\omega| < 0.2$ eV. The dashed curves are guides to the eyes obtained by tracking the Fermi crossings. (**b**) Experimental setup for polarization-dependent ARPES, and the odd symmetry of the 3*d*-orbitals with respect to the mirror plane. (**c**) Photoemission intensity $I(k, \omega)$ measured at 15 K along the cut #1 in the Γ-X direction. [(**d**) and (**e**)] The temperature dependence of EDCs at (**d**) X point and (**e**) Γ point. (**f**) The intensity change of the β band as a function of temperature. The peak intensity is obtained by integrating the spectral weight of the EDCs over a window of $1.0 < |\omega| < 2.9$ eV after subtracting a phenomenological linear background. Then, the peak intensity is normalized by the value of maximum and minimum intensity. Temperature dependence of the 4*f*-electron contribution to the volume thermal expansion $(\Delta V/V)_{4f}$ is also shown as red open circles on the right axis [4].

Previous photoemission spectroscopy measurements for Yb compounds have revealed that the Kondo resonance peak near E_F abruptly rises below the temperature of valence transition [6]. This intensity variation has been attributed to the hybridization between the conduction and Yb 4*f* electrons [6,7]. Although the peak energy of the β band is far below that of the Kondo resonance peak in Yb compounds, the result presented in this study may be derived from the strong hybridization between Ni 3*d* and Eu 4*f* states. Such hybridization leads to a reduction of the 4*f* electrons, and result in the heavy fermion and the valence fluctuating state approaching the trivalent Eu configuration at low temperatures [2,3,4].

In summary, we have studied electronic structure of $EuNi_2P_2$. ARPES data taken with the *s*-polarized photons reveal one hole-like Fermi surface around the X point. The spectral weight of Ni $3d_{xy}$ and/or d_{yz} band rapidly grows with decreasing temperatures, and its behavior is consistent with the intensive shrinkage of the $(\Delta V/V)_{4f}$ at low temperature. Our results suggest that the strong hybridization effect plays an essential role for the heavy fermion state in $EuNi_2P_2$.

References

[1] S. Tsutsui *et al.*, Phys. Rev. B **80**, 235115 (2009).
[2] R. Nagarajan *et al.*, Phys. Rev. B **32**, 2846 (1985).
[3] R. A. Fisher *et al.*, Phys. Rev. B **52**, 13519 (1995).
[4] Y. Hiranaka *et al.*, J. Phys. Soc. Jpn. **82**, 083708 (2013).
[5] S. Danzenbächer *et al.*, Phys. Rev. Lett. **102**, 026403 (2009).
[6] K. Yoshikawa *et al.*, Phys. Rev. B **72**, 165106 (2005).
[7] H. Sato *et al.*, J. Phys. Conference Series **592**, 012016 (2015).

Observation of Quantum Well States in Pd(100) Ultra Thin Films with ARPES

S. Sakuragi[a], E. F. Schwier[b], H. Iwasawa[b], M. Zheng[c], Y. Kojima[c], S. Nakahara[a], K. Shimada[b], H. Namatame[b], M. Taniguchi[b, c], and T. Sato[d]

[a] *Graduate School of Science and Technology, Keio University, Hiyoshi Yokohama 223-8522, Japan*
[b] *Hiroshima Synchrotron Radiation Center, Hiroshima University, Higashi-Hiroshima 739-0046, Japan.*
[c] *Graduate School of Science, Hiroshima University, Higashi-Hiroshima 739-8526, Japan.*
[d] *Department of Applied Physics and Physico-Informatics, Faculty of Science and Technology, Keio University, Hiyoshi, Yokohama 223-8522, Japan.*

Keywords: Pd, thin film, quantum-well states, magnetism, Stoner's criterion

In the last decade, the spontaneous magnetization appearing in nanosized metals which are nonmagnetic in the bulk shape has been reported. From the stand point of Stoner's criterion, this phenomenon is explained that the increase in the density of states near Fermi energy occurs by nanoscaling in metals. Recently, we investigated the magnetism of Pd(100) thin films by magnetic measurements and X-ray magnetic circular dichroism [1], motivated to the findings that the large spontaneous magnetization appeared from the topmost 2 - 5 layers on (100) facets of the Pd nanoparticles [2]. We found the ferromagnetism appearing in Pd(100) ultra thin films with 3 - 5 nm thickness where the magnetization periodically changed dependent on the film thickness. From the comparison with the theoretical calculations, this oscillating behavior is explained by the confinement of Pd's 4 *d* electrons in the film, i.e., the quantum-well states [3].

Angle-resolved photoemission spectroscopy (ARPES) is a powerful means to reveal the band dispersions of materials and thus discuss quantum-well states directly [4]. In this study, we performed in-situ ARPES measurement of the Pd(100) ultra thin film in order to clarify the origin of the ferromagnetism in Pd(100) based on the observation of discretization in the electric states of Pd due to the quantum-well states in the band dispersions.

Pd were deposited on $SrTiO_3$ (STO) substrate by 3 steps growth method [1] in HiSOR beamline BL-1 preparation chamber lower than 1×10^{-9} Torr of base pressure, and we measured in-situ ARPES. The film quality was checked using Auger electric spectroscopy, reflection high energy electron diffraction (RHEED), and low energy electron diffraction (LEED). After ARPES measurement, we checked the thickness of the films using ex-situ X-ray refraction measurement. Figs. 1(a) and 1(b) show the RHEED and LEED images of Pd(100) ultra thin film with the thickness of 3.8 nm. Based on the sharp streak lines in RHEED image and the clear four-hold spots in LEED image, we determined that the sample was fully (100) oriented.

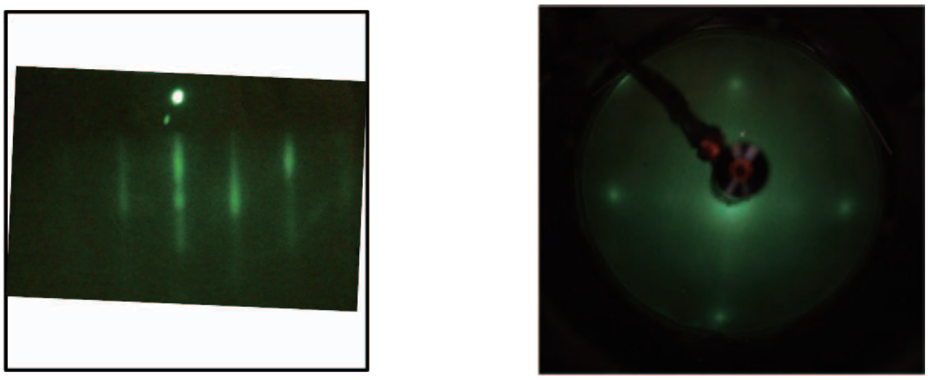

FIGURE 1. RHEED and LEED images of the Pd(100) ultra thin film with the thickness of 3.8 nm. (a) The RHEED image under the electron energy of 15 keV. The sharp streak lines originating from the flatness surface. (b) The LEED image under the electron energy of 60 eV. The (10) spots show that the sample is (100) oriented Pd film.

Figure 2 (a) shows the result of ARPES measurement around the Γ *K* direction of the Pd(100) ultra thin film taken at *hv* = 54 eV with the *p*-polarization geometry at the temperature of 270 K. Because the charge up occurred at low temperatures, we could measure ARPES only around the room temperature, and thus, the band dispersions in ARPES was broad. The wide band dispersions in ARPES made difficult to precisely discuss the electric states, thus we cannot discuss deeply in this data.

Both in Fig. 2(a) and the energy distribution curve at the Γ point [Fig. 2(b)], we observe the two band dispersions. The dispersion around -1.5 eV originates from Σ_1 band from the comparison with the ARPES measurement of bulk Pd [5]. On the other hand, the dispersion around -0.5 eV is not observed in bulk Pd. Thus, this band dispersion is attributed to electronic state peculiar to the nanoscaling of Pd, i.e. quantum-well states or surface states, and so on. Measuring the thickness dependent ARPES is required to reveal the origin of this dispersion.

In this beam time, we performed the in-situ ARPES measurements of Pd(100) ultra thin films and observed the peculiar band dispersion . Hence, we have plan to perform ARPES measurement of Pd films on the Nb doped STO(100) substrate or Cu(100) single crystal substrate [6] to suppress the charge up, and discuss the data in detail to clarify the origin of ferromagnetism in Pd(100) ultra thin films.

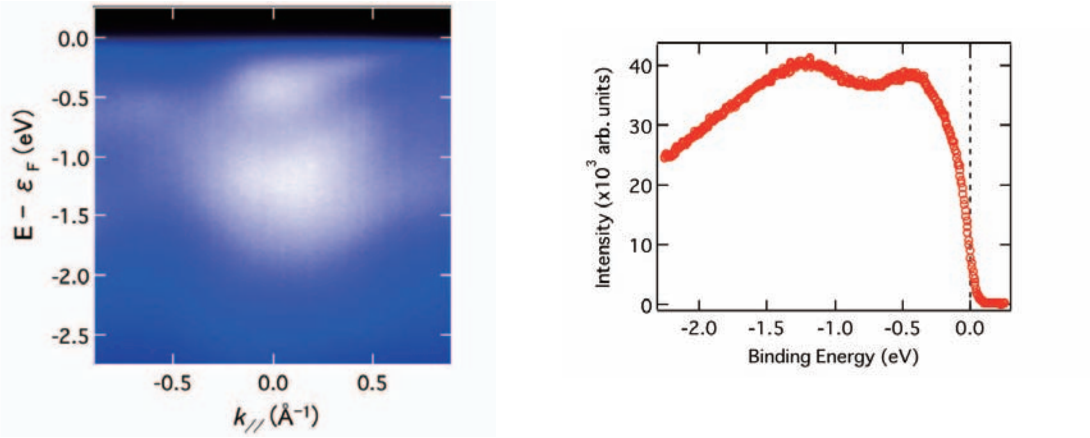

FIGURE 2. ARPES measurement results of the Pd(100) ultra thin film taken at *hv* = 54 eV at 270 K. (a) The image plots are shown around Γ *K* direction with the *p*-polarization geometry. (b) The energy distribution curve at the Γ point. The peculiar band dispersion of the Pd(100) ultra thin film was observed.

REFERENCES

1. S. Sakuragi et al., *Phys.Rev. B* **90**, 054411 (2014).
2. T. Shinohara, T. Sato and T. Taniyama, *Phys. Rev. Lett.* **91**, 197201 (2003).
3. S. C. Hong, J. I. Lee, and R. Wu, *Phys. Rev. B* **75**, 172402 (2007).
4. T.-C. Chiang, *Surf. Sci. Rep.* **39**, 181 (2000).
5. H. Hayashi et al., *Phys.Rev. B* **87**, 035140 (2013).
6. S. K. Saha et al., *Phys.Rev. B* **90**, 081404(R) (2014).

14-A-29 BL-1

Final State Effect on the Intensity Distribution in Angle-Resolved Photoelectron Spectroscopy for Epitaxial Graphene: A Study Using the Variable Polarized Photon

Shin-ichiro Tanaka[a]

[a] *Institute of Scientific and Industrial Research, Osaka University,*
Ibaraki 567-0047, Japan

Keywords: Graphene, ARPES, Linear Polarization

The π-band of the graphene makes the Dirac cone where the energy is linearly dispersed as a function of the electron momentum. The wavefunction of the π-band is described by a simple formula including the term of $\exp(i\theta_q)$, where θ_q is the angle around the K point in the reciprocal lattice space.[1] Therefore, graphene is one of the simplest and most suitable systems for studying a problem concerning the phase in the condensed matter physics, e.g., the Berry's phase. From this point of view, a number of the angle-resolved photoelectron spectroscopy (ARPES) studies were carried out to investigate the photoelectron intensity distribution depending on the linear and circular polarization of the incident photons.[1] However, in the studies so far, the polarization was only changed in two extreme cases; e.g., s-polarization and p-polarization in the case of the linear polarization. Here we examined the photoelectron intensity distribution from the Dirac cone as a function of the variable polarization angle ϕ, and found this factor strongly depends on the photon energy.

The experiments were carried out at the BL-1 of HiSOR, where the polarization angle can be varied at any value from the s-pol to p-pol by rotating the analyzer chamber equipped with the electron analyzer. The single-layered epitaxial graphene on SiC substrate was used and temperature during the measurement was 100K. Fig. 1(a) shows the experimental geometry and photoelectrons emitted along the *xz*-plane were taken in the ARPES spectra and it corresponds to dispersion measurement in the thick line in the Brillouin zone of the graphene shown in Fig. 1(b). The left panels of Figs. 2(a) and 2(b) show a series of the ARPES color maps when the polarization angle was changed from 0 (p-pol) to 90 (s-pol) degrees taken at the photon energy ($h\nu$) of 50 eV and 32eV, respectively. There are two nearly-linear branches due to the Dirac cone are shown, and only one of them is observed when the incident light is purely p-pol or s-pol light similarly to the previous work.[1] Hereafter the former and the latter are referred to as p- and s- branches, respectively. In angles between them, meanwhile, both are sometimes observed and the ratios in intensity of them depend on the polarization angle ϕ. It is obvious that this polarization-dependences are completely different for two different photon energies. In order to examine the polarization-dependence of the photoelectron intensity distribution in more detail, I introduce the asymmetry γ, which is defined as $\frac{I_p - I_s}{I_p + I_s}$, where I_p and I_s denote the photoelectron intensities of p- and s- branches in the MDC (momentum distribution curve) spectra at the Fermi level, and shown as dots in the right panels of Fig.2. By a simple analysis considering the magnitude of the electromagnetic field at the sample surface as a function of the photon incident angle ψ and the polarization angle ϕ, the asymmetry can be described by a simple formula as $\gamma = \frac{1-\alpha\tan^2\phi}{1+\alpha\tan^2\phi}$. Here, α is $\frac{M_y(h\nu)}{M_z(h\nu)\sin^2\psi + M_x(h\nu)\cos^2\psi}$, and M_z is the *x*-component of the transition dipole moments which is determined by the magnitude of the excitation matrix element such as $\langle \Psi_{f,k} | x | \Psi_{i,k} \rangle$, where the bra and ket are

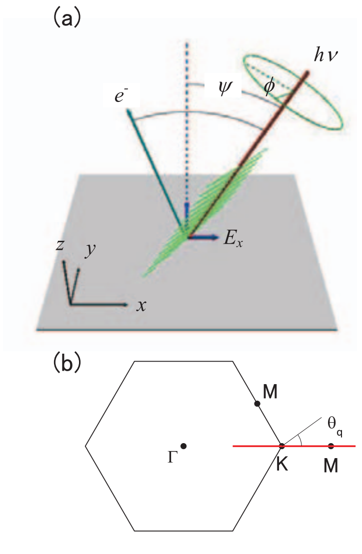

Fig.1 : Experimental geometry with a measured line in ARPES.

the final and initial states, respectively, of the photoexcitaion with the moment k. Similar relations hold for y and z. The final state is changed with changing the photon energy $h\nu$, thus M may be changed with $h\nu$. The lines in right panels in Figs. 2 (a) and (b) is the fitted curves using the above formula where α is only the adjustable parameter, and obtained a was 0.025 and 0.7 at $h\nu$=50 and 32 eV, respectively. The experimental results evidently show α and thus the ratio of the matrix elements among x, y and z axes depend on the photon energy. For studying the photon energy dependence in more detail, the asymmetry at a fixed ϕ was measured as a function of the photon energy. Figure 3 (a) shows the asymmetry γ measured at ϕ=45° for the photon energy region from 25 eV to 45 eV and that measured at ϕ=80° from 42 eV to 68 eV. Since the analyzer was fixed with respect to the photon beam and had a limited angle range for the incoming electron, the angle of the incidence has to be changed when the photon energy is widely changed as shown in Fig. 3(b). Fig. 3(c) plots α obtained from the asymmetry γ. Note that value of α depends on the photon incident angle ψ/

The obtained result is rather surprising. The magnitude of α changed in two orders with changing the photon energy from 25 to 60eV. Moreover, a sharp and strong dip is observed at hν=45.9eV. This strongly suggests that the assumption of the free-electron-like final state, which is usually used in the ARPES studies so far, is not in fact appropriate when the photoelectron intensity is taken into account. Rather, the empty states (bands) determined by the potential of the graphene has to be considered. The comparison with the theoretical calculation will lead a fruitful result.

(a) hν=50eV

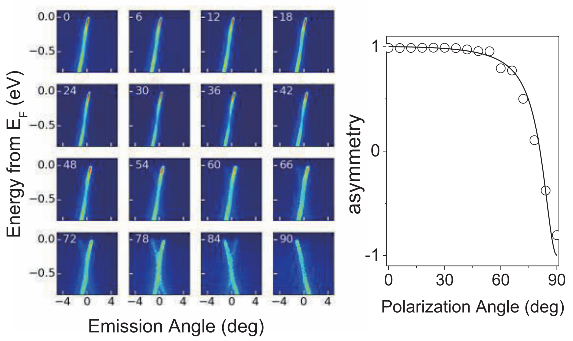

(b) hν=32eV

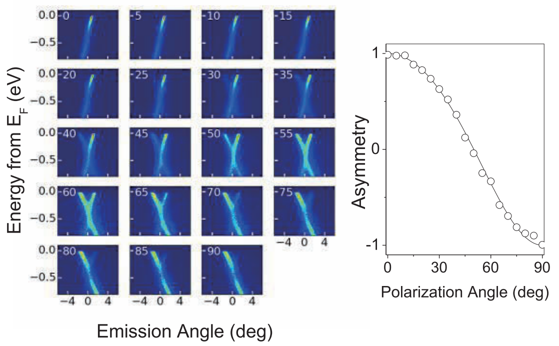

Fig. 2 : ARPES results (left) and the asymmetry of the photoelectron intensity at the Fermi level (right) taken at hν=50eV (a) and 32eV (b).

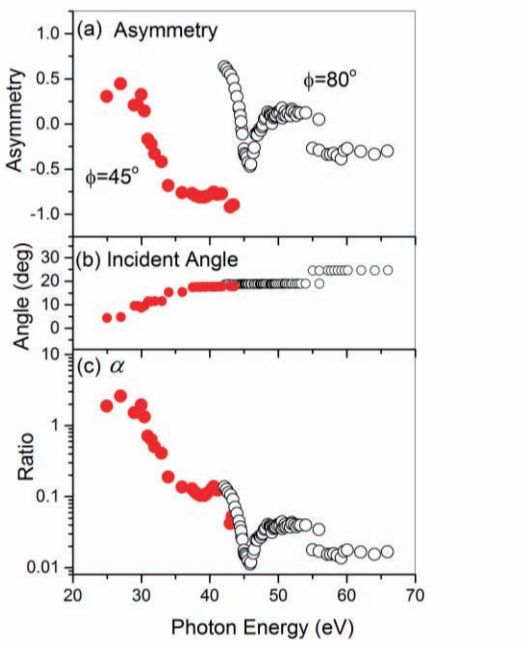

Fig. 3 : Asymmetry (a), incident photon angle (b), and the derived α (see texts) (c).

REFERENCES

1. M. Mucha-Kruczyński *et al.*, Phys. Rev. B 77, 195403 (2008); Y. Liu *et al.* Phys. Rev. Lett. 107 166803 (2011); I. Gierz *et al.* Phys. Rev. B 83 121408(R) (2011) ; C. Hwang *et al.*, Phys Rev. B 84 125422 (2011); I. Gierz *et al.*, Nano Lett. 12 3900 (2012);
2. Pourya Ayria and Riichiro Saito, private communication.

High-resolution angle-resolved photoemission study of Fe/MgO(100)

Mingtian Zheng[a], Eike F. Schwier[b], Koji Miyamoto[b], Taichi Okuda[b],
Kenya Shimada[b], Hideaki Iwasawa[b], Taiki Horike[a], Yorito Nagata[a],
Yohei Kojima[a], Hirofumi Namatame[b], and Masaki Taniguchi[a,b]

[a]*Graduate School of Science, Hiroshima University, Higashi-Hiroshima 739-8526, Japan*
[b]*Hiroshima Synchrotron Radiation Center, Hiroshima University, Higashi-Hiroshima 739-0046, Japan*

Keywords: Fe(100)-*p*(1×1)-O surface, Fermi surface, surface states

The oxygen adsorbed iron surface, Fe(100)-*p*(1×1)-O (O-Fe), is stable and used as a target material for the high-efficiency spin detector [1-3]. While the scattering properties of the surface have been examined [4,5], the Fermi surfaces and electronic band dispersions have not been revealed in detail so far. The physical properties of O-Fe is closely related to the *p-d* hybridization at surface [5-7]. It is important, therefore, to reveal the surface-derived states on Fe(100). The surface resonance states on pure Fe(100) and O-Fe have been examined by spin-resolved or spin-integrated angle-resolved photoemission spectroscopy (ARPES) [7-11]. However, information on the Fermi surfaces and band dispersions in thorough surface Brillouin zone (SBZ) with higher energy and momentum resolutions are still missing.

In this study, we have successfully performed high-resolution ARPES experiments of both pure Fe and oxygen adsorbed O-Fe thin films grown on MgO(100). All experiments were done at HiSOR BL-1. Single crystalline Fe(100) films were prepared on cleaned MgO(100) substrates using electron beam evaporator under ultrahigh vacuum conditions. Fig. 1(a) shows the LEED image of pure Fe(100) on MgO(100). The oxygen adsorbed O-Fe surfaces were prepared in a similar way as the VLEED targets, about 100 L O_2 was exposed on the Fe(100) film at room temperature, and then by flash heating at 900 K the O-Fe surface was obtained [1]. Fig. 1(b) shows the sharp 1×1 LEED pattern of O-Fe.

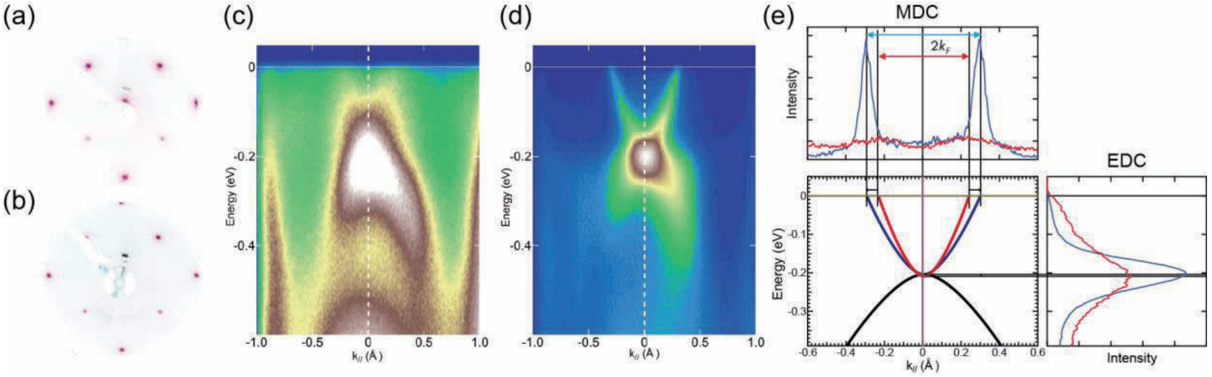

FIGURE 1. LEED patterns of: (a) pure Fe(100) before oxygen adsorption and (b) oxygen adsorbed Fe(100)-p(1×1)-O. Band dispersions close to Fermi edge (E_F) along $\bar{\Gamma}$-$\bar{X}$ direction at hν = 55 eV: (c) pure Fe(100) film before oxygen adsorption and (d) oxygen adsorbed Fe(100)-*p*(1×1)-O surface. (e) The schematic band dispersion evaluation close to E_F before (red) and after oxygen adsorption (blue).

Figs. 1(c) and 1(d) show the ARPES image plot around the $\bar{\Gamma}$-point near E_F of pure Fe(100) and O-Fe, respectively. One can see that the linewidth of O-Fe is narrower than that of pure Fe. This suggests that the scattering rate of electrons is reduced for O-Fe surface. Based on the sharper LEED pattern for O-Fe, we assume that the surface quality becomes better after the oxygen absorption. Furthermore, we can consider the reduction of the electron-electron interaction.

Fig. 1(e) shows the evaluated band dispersions close to E_F before (red) and after oxygen adsorption (blue). The MDC width at E_F is narrower after oxygen deposition, while $2k_F$ increases. We have evaluated $2k_F = 0.466$ Å for pure Fe, and $2k_F = 0.588$ Å for O-Fe; the Lorentzian width of pure Fe and O-Fe are 0.058 Å and 0.008 Å, respectively. Broader MDC linewidth at E_F indicates larger electron-defect scattering. The EDCs at $\bar{\Gamma}$-point clearly show the linewidth becomes narrower after oxygen adsorption. The EDC peak pure Fe is at -0.210 eV with the peak width of 0.162 eV. The peak position of O-Fe is -0.205 eV with the width of 0.052 eV.

Figs. 2(a)-(d) show the measured Fermi surface mapping around $\bar{\Gamma}$ point of pure Fe and O-Fe with the *p*- and *s*-polarization geometries taken at hν=55 eV. While the Fermi surfaces become sharper and clearer after oxygen adsorption, there exist similarities between pure Fe and O-Fe. In Figs. 2(b) and 2(d), there are several square-like Fermi surfaces around the $\bar{\Gamma}$ point of the SBZ for O-Fe. Corresponding features can be found in Figs. 2(a) and 2(c) for pure Fe.

We found that major spectral features around the $\bar{\Gamma}$ and $\bar{M}$ points did not change depending on the incident photon energies for Fe and O-Fe, suggesting that these bands are surface-derived.

We examined the band dispersion around $\bar{M}$ point with improved energy resolution, and found that two kinks exist at -75 meV and -20 meV in the energy band dispersion.

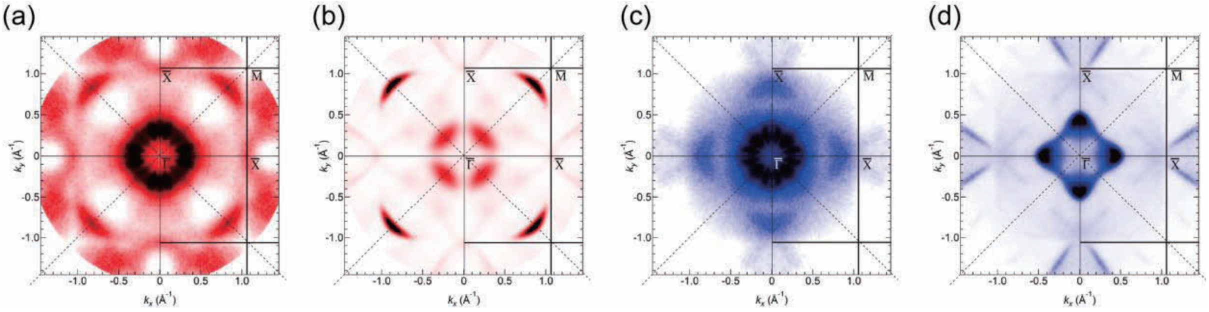

FIGURE 2. Fermi surface mapping of around $\bar{\Gamma}$ point at hν=55 eV of: (a), (b) pure Fe and O-Fe taken with *p*-polarization geometry, respectively, and (c), (d) with *s*-polarization geometry, respectively. There existed square-like Fermi surfaces around $\bar{\Gamma}$ point.

REFERENCES

1. R. Bertacco, M. Merano, and F. Ciccacci, Appl. Phys. Lett. 72, 2050 (1998).
2. R. Bertacco, M. Marcon, G. Trezzi, L. Duò, and F. Ciccacci, Rev. Sci. Instrum. 73, 3867 (2002).
3. T. Okuda et al., Rev. Sci. Instrum. 82, 103302 (2011).
4. F. Donati et al., Phys. Rev. B 79.195430 (2009).
5. A. Tange et al., Phys. Rev. B 81, 195410 (2010).
6. P. D. Johnson et al., Phys. Rev. Lett. 61.2257 (1988).
7. A. Clarke et al., Phys. Rev. B 41, 9659 (1990).
8. A. M. Turner, Yu Jeng Chang, and J. L. Erskine, Phys. Rev. Lett. 48, 348 (1982).
9. A. M. Turner, and J. L. Erskine, Phys. Rev. B 28, 5628 (1983).
10. E. Vescovo, O. Rader, and C. Carbone, Phys. Rev. B 47.13051 (1993).
11. L. Plucinski et al., Phys. Rev. B 80, 184430 (2009).

High-resolution ARPES of Ce thin films Ⅱ

Y. Kojima[a], K. Shimada[b], Y. Nagata[a], E. F. Schwier[b], H. Iwasawa[b], T. Horike[a],
M. Zheng[a], Y. Aiura[c], H. Namatame[b], M. Taniguchi[a, b]

[b]*Graduate School of Science, Hiroshima University, Higashi-Hiroshima 739-8526, Japan*
[b]*Hiroshima Synchrotron Radiation Center, Hiroshima University, Higashi-Hiroshima 739-0046, Japan*
[c]*National Institute of Advanced Industrial Science and Technology, Tsukuba, Ibaraki 305-8568, Japan*

Keywords: Cerium, 4f electron, *c-f* hybridization, ARPES.

In the rare earth metals, the interaction between highly localized 4*f*-electrons and itinerant conduction electrons (*c-f* hybridization) plays an important role for various physical properties such as the Kondo effect, RKKY interaction, heavy fermion [1]. In order to understand unusual physical properties of the rare earth metals, it is important to experimentally elucidate the quasiparticle properties in the *c-f* hybridized bands near the Fermi level (E_F).

As a typical example of the heavy fermion system, here we study the electronic band structure and Fermi surface of a single crystalline Cerium (Ce) thin film by means of high-resolution angle-resolved photoemission spectroscopy (ARPES). The electronic structure of Ce is relatively simple because nominally one 4*f* electron exists in the valence band. It has been reported that an epitaxial growth of Ce film is possible on W(110) [2][3][4][5].

High-resolution ARPES measurements were carried out on the linear undulator beamline BL-1 of HiSOR. A clean surface of W(110) substrate was prepared by repeated cycles of heating in an oxygen atmosphere (5×10^{-9} Torr) at 1200 K and a subsequent flash to 2000 K. Ce thin film was deposited on the W(110) substrate using the electron-beam evaporator. We characterized cleanness and thickness of the Ce thin films by Auger electron spectroscopy (AES). The level of impurities at surface was below the detection limit of AES, and the thickness of the film was evaluated to be 5.1 monolayers [6]. We observed sharp 1×1 low energy electron diffraction spots exhibiting high quality of the prepared sample surface [2]. The sample was mounted on the 6 axes He cryostat and the temperature was set at 11 K during ARPES measurements.

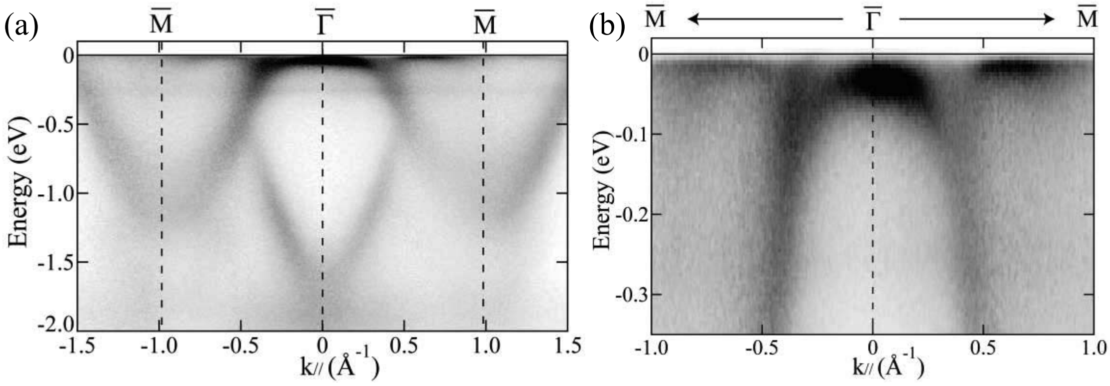

Figure 1. ARPES image plot of Ce/W(110) taken at hν = 42 eV at temperature of 11 K. Black portions represent higher spectral intensity. (a) Band dispersion of $\overline{\Gamma}\overline{\mathrm{M}}$ direction. (b) spectral features near E_F.

Figure 1 (a) is the ARPES image plot with an incident photon energy of hν = 42 eV. One can see dispersive parabolic bands with energy bottom at the $\overline{\Gamma}$ point (-1.8 eV) and the $\overline{\mathrm{M}}$ point (-1.3 eV). Based on the photoionization cross-section, and results from the resonant photoemission spectroscopy, we assume that these dispersive bands are derived from the Ce 5*d* state. We can also observe flat bands near E_F, -0.25 eV and -1.9 eV.

Based on the 4*d*-4*f* resonance photoemission spectroscopy, we can conclude that these structures are derived from the Ce 4*f* state. In Fig. 1(b), one can clearly see a flat band at E_F at $|k_{//}| \sim 0.5$ Å^{-1}. The hole-like band located just below E_F at the $\overline{\Gamma}$ point has a large effective mass. The distance between Ce atoms is estimated to 3.67 Å from measured $|k_{\overline{\Gamma M}}|$. It is larger than 3.43 Å for the bulk α-Ce, and close to 3.65 Å for the bulk γ-Ce.

Figure 2 (a) shows the temperature dependent ARPES image plot of Ce/W(110) near E_F taken at hν = 42 eV. At low temperature (11 K and 50 K), one can see flat bands located near E_F at $|k_{//}| \sim 0.5$ Å^{-1}. Figure 2(b) shows EDC intensity at $k_{//} = 0.6$ Å^{-1} (arrows in Fig. 2(a)) divided by the Fermi-Dirac function for each temperature. We found that the spectral intensity at E_F is enhanced between 50 K and 100 K, indicating the existence of the characteristic temperature between 50 K and 100 K.

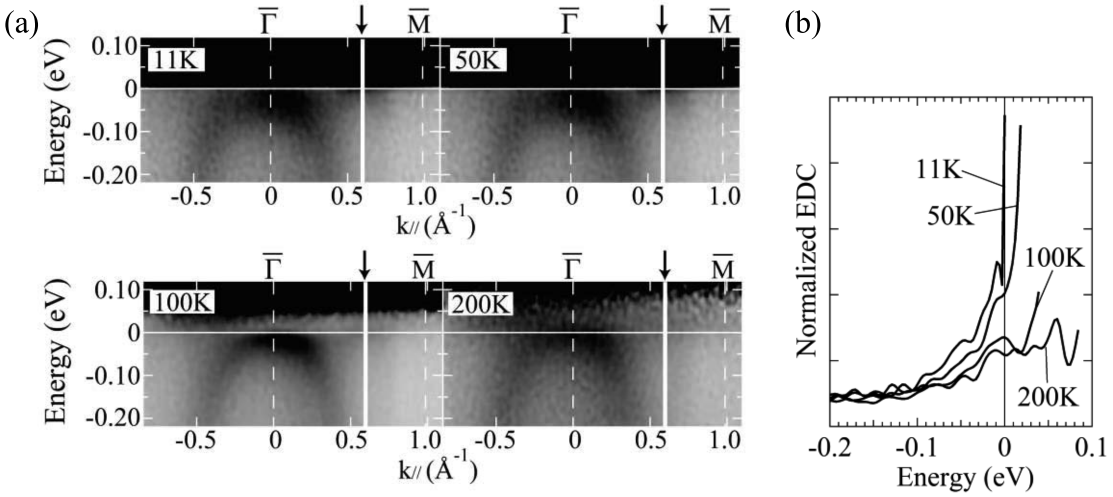

Figure 2. (a) Temperature-dependent ARPES image plot of Ce/W(110) taken at hν = 42 eV. (b) Temperature-dependence of the normalized EDC at $k_{//} = 0.6$ Å^{-1} (arrows in 2(a)).

REFERENCES

[1] K. Yamada, *Electron Correlation in Metals* (Cambridge University Press, 2004).
[2] C. Gu et al., Phys. Rev. Lett., **67**, 12, 1622 (1991).
[3] E. Weschke *et al.*, Phys. Rev. B **58**, 3682 (1998).
[4] F. Schiller et al., Phys. Rev. B, **68**, 233103 (2003).
[5] O. Morimoto et al., Surf. Sci., **603**, 2145-2151 (2009).
[6] D. Tian *et al.*, Phys. Rev. B **45**, 3749 (1992).

ARPES study on anomalous kinks in σ bands of graphene

Sung Won Jung[a,b], Yeongsup Sohn[a,b] and Keun Su Kim[a,b]

[a]*Department of Physics, Pohang University of Science and Technology, Pohang 790-784, Korea*
[b]*Center for Artificial Low Dimensional Electronic Systems, Institute for Basic Science, Pohang 790-784, Korea*

Keywords: Kink, graphene, angle-resolved photoemission spectroscopy

Graphene has served as a prototypical model system for study of various low-dimensional physics [1]. It has rather simple lattice and electronic structures, and the energy scale of phonons, collective excitations of periodic atoms, is relatively large (~200 meV), making it ideal to investigate the electron-phonon interaction in low dimensions [2]. Angle-resolved photoemission spectroscopy (ARPES) is a powerful technique, which can not only directly visualize energy versus momentum dispersion of electrons, but also identify a signature of electron-boson interaction, an abrupt slope change in dispersion (kink) [2,3]. It has been reported that ARPES spectra of π bands in graphene indeed show such kinked dispersion in the energy scale of 150~180 meV from the Fermi level, which is typical of optical phonons in graphene [4,5].

Recently, it was newly observed that the σ bands of graphene, having a binding energy higher than 4 eV, exhibit a similar kinked dispersion [6]. This is rather surprising, given that the electron-boson kinks typically occur at low energies from the Fermi level, and has not been observed in such high binding energy [3]. The observed kink structure was attributed to a signature of electron-phonon interaction [6], but its microscopic origin remains unclear. Another point of interest is the energy value of this kink structure, determined by the energy scale of involved boson modes). The π bands kink typically shows ~150 meV, consistent with the optical phonon mode at the zone boundary [4,5], while the kink of sigma-bands has about 200 meV, which corresponds to the optical phonon mode at the zone center [6]. This implies a unique electron-phonon correlation in graphene that the photoholes in π bands favor the intervalley scattering, while those in sigma bands favor the intravalley scattering.

To clarify this issue, we have performed a systematic ARPES investigation in HiSOR BL1. The sample was quasi-freestanding graphene grown on the surface of hydrogen-terminated silicon carbides. Our angle-resolved photoemission (ARPES) spectra of graphene σ bands with the photon energy of 30~40 eV show anomalous kinks at high energies as shown in Figure 1 below. The spectral features are overall consistent with the previously reported data [6]. However, we additionally found inner and outer σ bands show a strong out-of-phase spectral modulation with vanishing intensity near their vertex [7]. Such characteristic intensity patterns are thought to be due to quantum interference of electronic wavefunctions coming from two symmetric sublattices of graphene. We have attempted spectral simulations based on sublattice interference, which reproduce apparent kink features without involving any coupling of bosonic excitations [7]. This result identify the mechanism leading to kink features in σ bands of grphaene, which can also explain the origin of high-energy kinks observed in other correlated materials systems.

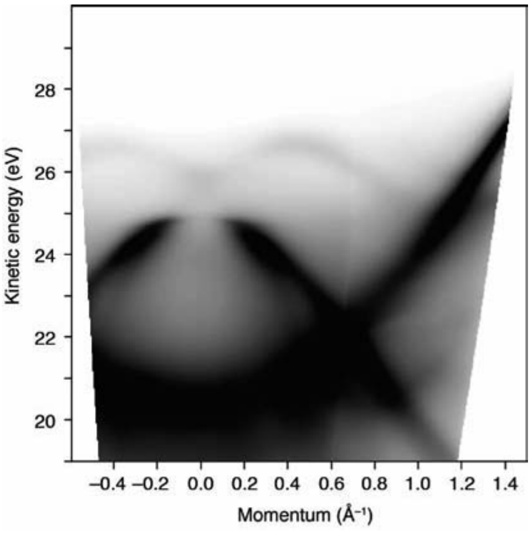

FIGURE 1. Angle-resolved photoemission spectra of graphene σ bands, taken with the photon energy of 34 eV.

REFERENCES

1. A. H. Castro Neto *et al.,* Review of Modern Physics **81,** 109 (2009).
2. C. S. Leem *et al.,* Physical Review Letters **100,** 016802 (2008).
3. A. Damascelli *et al.,* Review of Modern Physics **75,** 473 (2003).
4. A. Bostwick *et al.,* Nature Physics **3,** 36 (2007).
5. S. Y. Zhou *et al.,* Physical Review B **78,** 193404 (2008).
6. F. Mazzola *et al.,* Physical Review Letters **111,** 216806 (2013).
7. S. W. Jung *et al., to be submitted.*

14-B-18 BL-1

Polarization-Dependent Study of ARPES Spectral Intensity of $Ba(Fe_{1-x}Co_x)_2As_2$

H. Takita[a], N. Kishimoto[a], Y. Nakashima[a,b], W. Mansuer[a], A. Ino[a,b], M. Arita[c],
H. Namatame[c], M. Taniguchi[a,c], Y. Aiura[b,d], I. Hase[b,d], H. Eisaki[b,d],
K. Kihou[b,d], C. H. Lee[b,d], A. Iyo[b,d], M. Nakajima[b,e], and S. Uchida[b,e]

[a]*Graduate School of Science, Hiroshima University, Higashi-Hiroshima 739-8526, Japan*
[b]*JST, Transformative Research-Project on Iron Pnictides (TRIP), Chiyoda, Tokyo 102-0075, Japan*
[c]*Hiroshima Synchrotron Radiation Center, Hiroshima University, Higashi-Hiroshima 739-8526, Japan*
[d]*National Institute of Advanced Industrial Science and Technology, Tsukuba 305-8568, Japan*
[e]*Department of Physics, University of Tokyo, Tokyo 113-0033, Japan*

Keywords : ARPES, Polarization dependence, Iron-pnictides

The ground state of iron-pnictides evolves from an antiferromagnetic (AF) phase to a superconducting (SC) phase in a way similar to that of cuprates. This suggests that electronic correlation in the iron-pnictides is strong enough to support the high critical temperature of superconductivity. On the other hand, a significant difference between iron-pnictides and cuprates is in the orbital degree of freedom. While the low-energy electronic structure of cuprates is described only by the $d_{x^2-y^2}$ orbital, that of iron-pnictides involves all of the 3d orbitals. As a result, multiple branches of band dispersion are present near the Fermi level, and they form several sheets of Fermi surface with various orbital characters. The orbital degree of freedom has been considered as the key to understanding the electronic correlation in the iron-pnictides.

Polarization-dependent angle-resolved photoemission spectroscopy (ARPES) is a powerful tool for studying the multi-orbital band structure in iron-pnictides. Owing to the dipole-selection rule for the photoemission process, the photoemission intensity is vitally dependent on the spatial symmetry of the electronic wave function in solids and the polarization of the incident light. Specifically, when the polarization of the incident light is perpendicular (parallel) to the detection plane, which is defined as the plane including the surface-normal and photoelectron-emission directions, the electronic states of odd (even) reflection parity about the detection plane are selectively observed.

In this study, we performed a polarization-dependent ARPES of $Ba(Fe_{1-x}Co_x)_2As_2$ (x = 0.02, 0.04) using the linearly-polarized light. High-quality single crystals of $Ba(Fe_{1-x}Co_x)_2As_2$ were grown by a self-flux method. The ARPES experiments were performed at BL-1 of HiSOR in Hiroshima Synchrotron Radiation Center. Whole of the measurement chamber is continuously rotatable around the photon-beam axis of BL-1. From a viewpoint of the sample, the polarization vector of incident photon is rotatable without changing the incident beam axis. The incident photon energy was set at $h\nu$ = 55 eV. All the measurements were performed at a low temperature of ~10 K and in vacuum better than 9×10^{-11} Torr.

Figure 1(a) shows the momentum distribution of the ARPES intensity around X point in the AF phase of $Ba(Fe_{0.96}Co_{0.04})_2As_2$. The angle of the polarization vector is 36° with respect to the Γ-X high-symmetry line. Because of the reflection symmetry about the Γ-X line in the AF phase of $Ba(Fe_{1-x}Co_x)_2As_2$, the band dispersion should be symmetric about the Γ-X line. This reflection symmetry is preserved in the geometry of our ARPES experiments, and indeed it has been established that the ARPES intensity distributions obtained with the p- and s-polarized light have reflection symmetry about the Γ-X line [1]. As shown in Fig. 1(a), however, the ARPES intensity distribution obtained with the mixture of p- and s-polarized light is asymmetric about the Γ-X line. For instance, the intensity around (k_x, k_y) = (1.1, -0.5) $Å^{-1}$ is lower than that around (k_x, k_y) = (1.1, 0.5) $Å^{-1}$. This implies that the relative phase between p- and s-polarized light plays a certain role in the ARPES intensity distribution. Figures 1(b) and 1(c) show the energy-momentum (E-k) plots extracted along the $k_x = 0.9$ Å^{-1} and $k_x = 1.47$ Å^{-1} lines, respectively. In the former cut, the intensity in $k_y < 0$ is higher than that in $k_y > 0$. In the latter cut, by contrast, the intensity in $k_y < 0$ is lower than that in $k_y > 0$. This contrast can also be seen from momentum distribution curves at E-E_F = -100, -125 and -150 meV, as shown in Fig. 1(d). The inversion of the asymmetry between the first and second Brillouin zones is consistent with the fact that the C_2 rotational symmetry is preserved in the collinear AF phase of $Ba(Fe_{1-x}Co_x)_2As_2$.

In summary, we observed the ARPES spectra of $Ba(Fe_{1-x}Co_x)_2As_2$ with some polarizations intermediate between the p- and s-polarizations. Although the momentum distribution of ARPES intensity drastically changes with the polarization angle, it remains consistent with the rotational symmetry preserved in the AF phase of the $Ba(Fe_{1-x}Co_x)_2As_2$. As for the present experiment, the excitation photons are limited to a couple of energies and some selected polarization angles. Therefore, further investigation is necessary for revealing the orbital texture in the iron-pnictides.

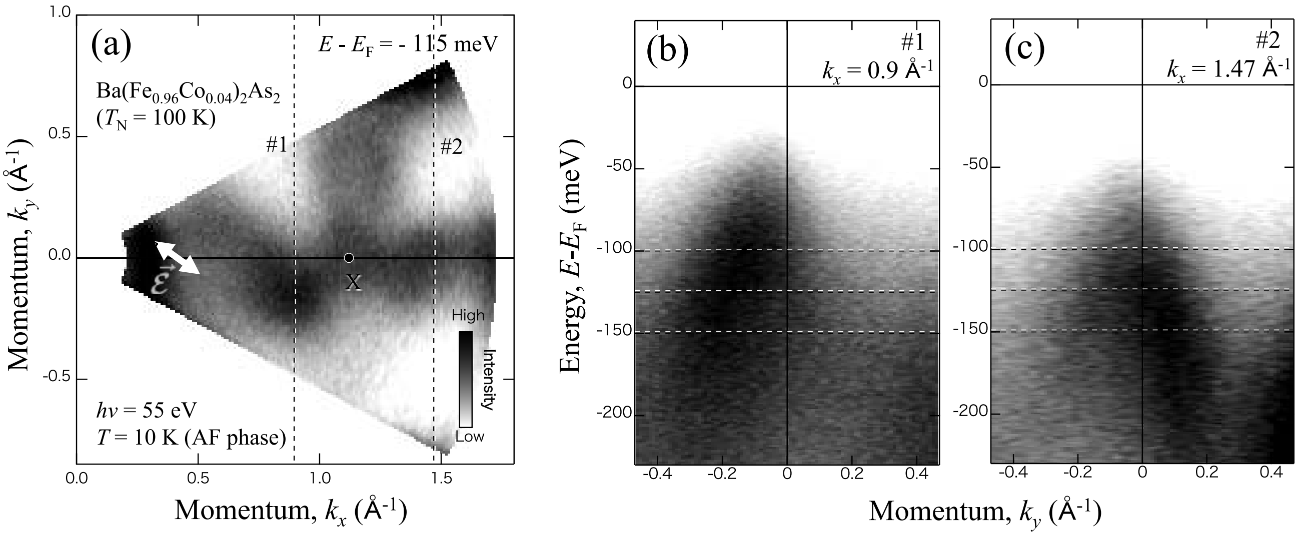

FIGURE 1 (a) Momentum distribution of ARPES intensity at $E - E_F$ = -115 meV for the AF phase of $Ba(Fe_{0.96}Co_{0.04})_2As_2$, taken with $h\nu$ = 55 eV at T = 10 K. The black area denotes high spectral intensity. The angle of polarization vector (white arrow) is 36° with respect to the Γ-X symmetry line. The intensity was integrated over an energy window of 20 meV. (b)(c) E-k plots extracted along the $k_x = 0.9$ Å^{-1} and $k_x = 1.47$ Å^{-1} lines, respectively. (d) Momentum distribution curves at energies of $E - E_F$ = -100, -125 and -150 meV. Filled and open circles denote the cut taken along the $k_x = 0.9$ Å^{-1} and $k_x = 1.47$ Å^{-1} lines.

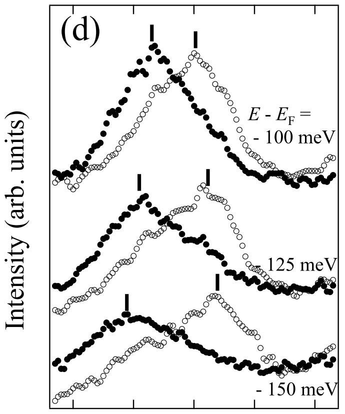

REFERENCE

1. Ming Yi *et al.*, *Proc. Nat. Acad. Sci*, **108,** 6878-6883 (2011).

Multi-band electronic structure of $CeO_{0.5}F_{0.5}BiS_2$

T. Mizokawa[a], T. Sugimoto[b], D. Ootsuki[c], M. Takahashi[c], N. L. Saini[d],
T. Asano[e], T. Nakajima[e], R. Higashinaka[e], T. Matsuda[e], Y. Aoki[e],
E. F. Schwier[f], M. Zheng[f], K. Kojima[f], H. Iwasawa[f],
K. Shimada[f], H. Namatame[f], M. Taniguchi[f,g]

[a] *Department of Applied Physics, Waseda University, Shinjuku-ku, Tokyo 169-8555, Japan*
[b] *Department of Complexity Science and Engineering, University of Tokyo, Kashiwa, Chiba 277-8561, Japan*
[c] *Department of Physics, University of Tokyo, Kashiwa, Chiba 277-8561, Japan*
[d] *Department of Physics, University of Roma "La Sapienza", Piazzale Aldo Moro 2, 00185 Roma, Italy*
[e] *Department of Physics, Tokyo Metropolitan University, Hachioji, Tokyo 192-0397, Japan*
[f] *HiSOR, Hiroshima University, Higashihiroshima, Hiroshima 739-0046, Japan*
[g] *Graduate School of Science, Hiroshima University, Higashihiroshima, Hiroshima 739-8526, Japan*

Keywords: Kondo physics, Ce 4*d*-4*f* resonance, BiS_2 superconductor

Since the discovery of superconductivity in the BiS_2 system by Mizuguchi *et al.* [1], the electronic structures of the BiS_2-based superconductors have been attracting great interest. Among the various BiS_2-based compounds, $CeO_{1-x}F_xBiS_2$ is very unique in that the superconductivity in the BiS_2 plane and the ferromagnetism in the $CeO_{1-x}F_x$ plane coexist for $x > 0.5$ [2]. Angle-resolved photoemission spectroscopy (ARPES) studies on superconducting $NdO_{1-x}F_xBiS_2$ and $LaO_{1-x}F_xBiSe_2$ have revealed that the Fermi pockets around X point of the Brillouin zone are constructed from the Bi $6p_x/6p_y$ orbitals and should be responsible for the superconductivity [3-5]. On the other hand, an x-ray absorption study on $CeO_{1-x}F_xBiS_2$ has indicated that the Ce valence is intermediate (valence fluctuation) and the Ce 4*f* states may contribute to the Fermi surfaces [6]. In order to identify the contribution of the Ce 4*f* states, we have performed Ce 4*d*-4*f* resonant angle-resolved photoemission spectroscopy on $CeO_{1-x}F_xBiS_2$ at BL-1, HiSOR.

The middle and right panels of Fig. 1 show the ARPES data taken at 120.7eV (on-resonance) and 115.4 eV (off-resonance), respectively, for $CeO_{0.5}F_{0.5}BiS_2$. The momentum k_x is running along the Γ-X direction of the Brillouin zone. The Bi 6*p* Fermi pocket around X point is observed in the off-resonance data. The valence band below -1 eV can be assigned to Bi 6*s*, S 3*p*, and Ce 4*f* bands. When the photon energy is tuned to the Ce 4*d*-4*f* absorption energy (120.7 eV), the flat band located at -1.5 eV is considerably enhanced indicating that the Ce 4*f* electrons are basically localized and do not contribute to the Fermi pockets around X. The energy distribution curve for the on-resonance photon energy exhibits an intense Ce 4*f* peak at -1.5 eV. The resonant ARPES results show that the Ce 4*f* band is located between the Bi 6*p* conduction band and the Bi 6*s*/S 3*p* valence band, and that there is no appreciable Ce 4*f* spectral weight at the Fermi level. Namely, $CeO_{0.5}F_{0.5}BiS_2$ belongs to the Kondo regime and the Ce valance should be 3+. This is consistent with the bulk sensitive Ce *L*-edge x-ray absorption results where $CeOBiS_2$ falls in the valence fluctuation regime and gradually changes to the Kondo regime with the F substitution for O [6]. The superexchange or RKKY interaction between the localized Ce 4*f* moments is derived from the Ce 4*f* – Bi 6*p* hybridization.

On the other hand, we found that the Ce 4*f* lineshape of $CeOBiS_2$ is very similar to that of $CeO_{0.5}F_{0.5}BiS_2$ and is different from that expected for valence fluctuating systems. In typical valence fluctuating systems such as $CeRu_2$, the Ce 4*f* band is strongly hybridized with the conduction band such as Ru 4*d* and is well reproduced by local density approximation (LDA) band calculations. The observed Ce 4*f* band of $CeOBiS_2$ has very flat dispersion and does not agree with the LDA band calculation [7]. This is inconsistent with the bulk sensitive Ce *L*-edge x-ray absorption results on $CeOBiS_2$ [6]. In addition, it is well established that Ce 4*d*-4*f* resonant photoemission is more surface sensitive than Ce 3*d*-4*f* resonant photoemission, and that the Ce 3*d*-4*f* resonance is more suitable to study the bulk valence fluctuating state of $CeRu_2$ [8]. The discrepancy in $CeOBiS_2$ can be assigned to the surface effect in which the Ce 4*f*-Bi 6*p* hybridization is reduced at the surface layer and the Ce 4*f* electrons are localized at the surface whereas the bulk Ce 4*f* electrons are rather itinerant. However, the Anderson impurity model (AIM) analysis of the Ce 4*f* core-level x-ray photoemission spectrum, which is also surface sensitive, is consistent with the AIM analysis of the bulk sensitive Ce *L*-edge spectrum, suggesting that the surface Ce 4*f* state would be similar to the bulk one. In order to resolve this problem, the Ce 4*d*-4*f* resonant ARPES and the Ce *L*-edge x-ray absorption should be measured on the same pieces of $CeO_{1-x}F_xBiS_2$ single crystal and should be analyzed using AIM or more realistic model calculations.

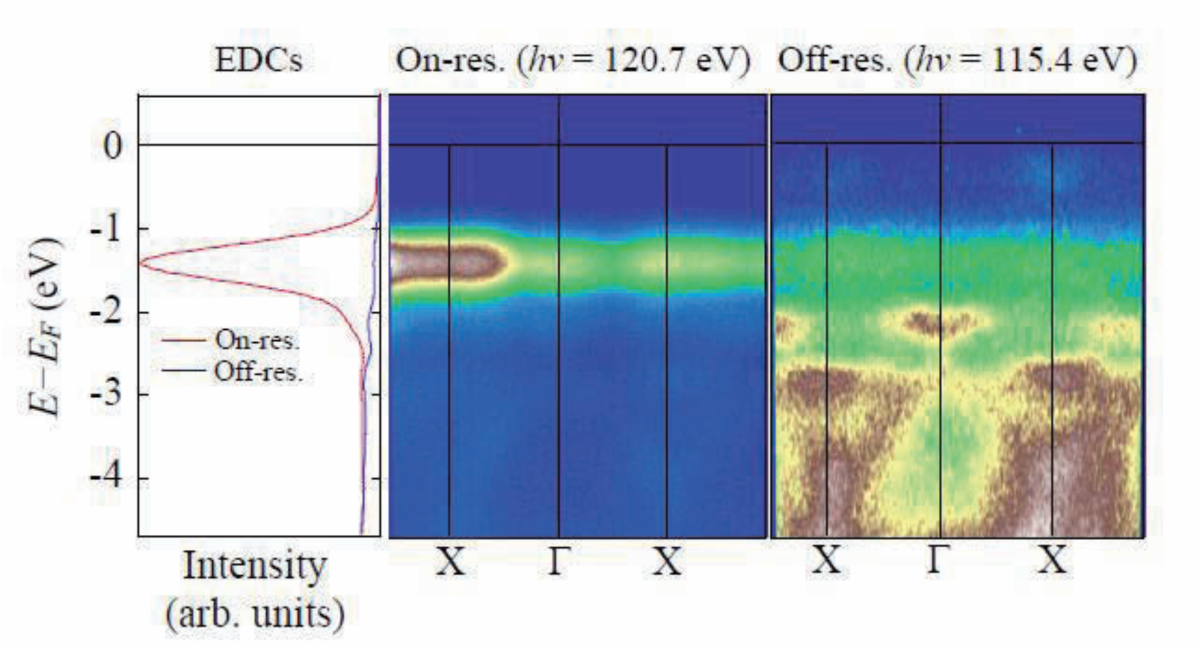

FIGURE 1. Right panel: ARPES spectra of $CeO_{0.5}F_{0.5}BiS_2$ along the Γ-X direction taken at 115.4 eV (off-resonance). Middle panel: ARPES spectra of $CeO_{0.5}F_{0.5}BiS_2$ along the Γ-X direction taken at 120.7 eV (on-resonance). Left panel: Energy distribution curves for the on- and off-resonance.

REFERENCES

1. Y. Mizuguchi, H. Fujihisa, Y. Gotoh, K. Suzuki, H. Usui, K. Kuroki, S. Demura, Y. Takano, H. Izawa, and O. Miura, Phys. Rev. B **86**, 220510(R) (2012).
2. S. Demura, K. Deguchi, Y. Mizuguchi, K. Sato, R. Honjyo, A. Yamashita, T. Yamaki, H. Hara, T. Watanabe, S. J. Denholme, M. Fujioka, H. Okazaki, T. Ozaki, O. Miura, T. Yamaguchi, H. Takeya, and Y. Takano, J. Phys. Soc. Jpn. **84**, 024709 (2015).
3. Z. R. Ye, H. F. Yang, D. W. Shen, J. Jiang, X. H. Niu, D. L. Feng, Y. P. Du, X. G. Wan, J. Z. Liu, X. Y. Zhu, H. H. Wen, and M. H. Jiang, Phys. Rev. B **90**, 045116 (2014).
4. L. K. Zeng, X. B. Wang, J. Ma, P. Richard, S. M. Nie, H. M. Weng, N. L. Wang, Z. Wang, T. Qian, and H. Ding, Phys. Rev. B **90**, 054512 (2014).
5. N. L. Saini, D. Ootsuki, E. Paris, B. Joseph, A. Barinov, M. Tanaka, Y. Takano, and T. Mizokawa, Phys. Rev. B **90**, 214517 (2014).
6. T. Sugimoto, B. Joseph, E. Paris, A. Iadecola, T. Mizokawa, S. Demura, Y. Mizuguchi, Y. Takano, and N. L. Saini, Phys. Rev. B 89, 201117(R) (2014).
7. T. Sugimoto, D. Ootsuki, M. Takahashi, C. Morice, E. Artacho, S. S. Saxena, E. F. Schwier, M. Zheng, Y. Kojima, H. Iwasawa, K. Shimada, M. Arita, H. Namatame, M. Taniguchi, N. L. Saini, T. Asano, T. Nakajima, R. Higashinaka, T. D. Matsuda, Y. Aoki, and T. Mizokawa, arXiv:1505.01969
8. A. Sekiyama, T. Iwasaki, K. Matsuda, Y. Saitoh, Y. Onuki, S. Suga, Nature **403**, 396 (2000).

Angle-resolved Photoelectron Spectroscopy Study of $Ce(Ru_{1-x}Fe_x)_2Al_{10}$

Y. Yamamoto[a], H. Yamaoka[b], E. F. Schwier[c], F. Tajima[d], T. Nishioka[d], H. Iwasawa[c], K. Shimada[c], H. Namatame[c], and M. Taniguchi[e,c], J. Mizuki[a],

[a]Graduate School of Science and Technology, Kwansei Gakuin University, Sanda, Hyogo 669-1337, Japan
[b]RIKEN SPring-8 Center, Sayo, Hyogo 679-5148, Japan
[c]Hiroshima Synchrotron Radiation Center, Hiroshima University, Higashi-Hiroshima, Hiroshima 739-0046, Japan
[d]Graduate School of Science, Kochi University, 2-5-1 Akebono, Kochi 780-8520, Japan
[e]Graduate School of Science, Hiroshima University, Higashi-Hiroshima, Hiroshima 739-0046, Japan

Keywords: electronic structure, photoelectron spectroscopy, Ce1-2-10

The ternary intermetallic compounds RT_2Al_{10}, where R is a rare earth and T one of the transition metals Ru, Os, or Fe, were discovered by Thiede *et al.* in 1998 [1]. In CeT_2Al_{10} antiferromagnetic (AFM) order occurs for T = Ru and Os at unusually high ordering temperatures (T_0 = 27.3 K and 28.7 K) and with fairly small ordered moments of $\mu \sim 0.40\ \mu_B$/Ce and 0.29 μ_B/Ce for T = Ru and Os, respectively [2]. $CeFe_2Al_{10}$ shows semiconducting behavior at low temperatures and does not exhibit magnetic order. Its temperature dependence rather suggests intermediate valent behavior due to hybridization of 4*f* and conduction electrons (*c*-*f*). The reason why T_0 is so anomalously large remains an unresolved problem. Usually the Kondo effect, i. e. the presence of *c*-*f* hybridization, suppresses the magnetic order. We therefore study systematically what impact the Kondo effect has on the transition temperature T_0. A measure for the *c*-*f* hybridization is the cerium valence which can be obtained from deviations of the lattice distances from Vegard's law, or more directly, from the electronic occupation of the 4*f* shell. However, our recent resonant x-ray emission spectroscopy (RXES) study showed a poor correlation between the suppression of the magnetic order and the valence fluctuation.[3] In $CeRu_2Al_{10}$ the ground state changes from local to valence fluctuate systems with pressure and also sudden disappearance of T_0 has been observed. Our RXES study of the pressure dependence for $CeRu_2Al_{10}$ also seemed to show a poor correlation between the T_0 and the hybridization [3]. These results motivated us to study the electronic structure by another way with angle-resolved photoelectron spectroscopy (ARPES), which can give us complementary information with the RXES.

Here we report preliminary results of our investigation of the band structure of CeT_2Al_{10} by means of DFT and ARPES. Figure 1 shows band dispersion of Ce *f* states, Al *p* states, and Ru *d* states of $CeRu_2Al_{10}$, which are the main orbital contributions to the electronic structure close to the Fermi energy.

The spin unpolarized calculations find the electronic structure of the valence band to be dominated by Ru *d* and some Al *p* states, while the conduction band shows strong Ce *f* character. Between the valence band and the conduction band our DFT calculations further predict a small energy range of less than 1 eV below the Fermi energy where a small number of *c*-*f* hybridized bands exist. The orbital weighted band

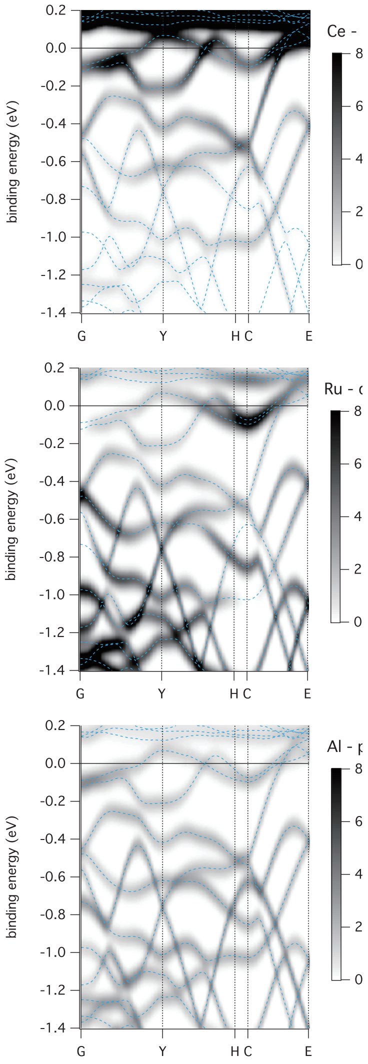

FIGURE 1. Band dispersion of Ce *f* states, Ru *d* and Al *p* states of $CeRu_2Al_{10}$ as calculated by DFT along selected high symmetry paths in the Brillouin zone.

structure further shows the strong *k*-dependence of the Ru contribution of the bands crossing the Fermi energy. The latter should be important for the electronic properties of this compound and its sister compounds CeT_2Al$_{10}$. Further investigation of the spin polarized band structure as well as a comparison with T = Fe, Os will be conducted.

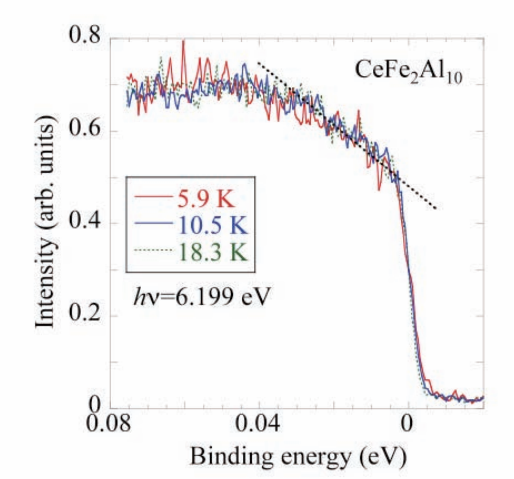

FIGURE 2. Valence band spectra of CeFe$_2$Al$_{10}$ at 5.9, 10.5, and 18.3 K with the laser light of $h\nu$ = 6.3582 eV.

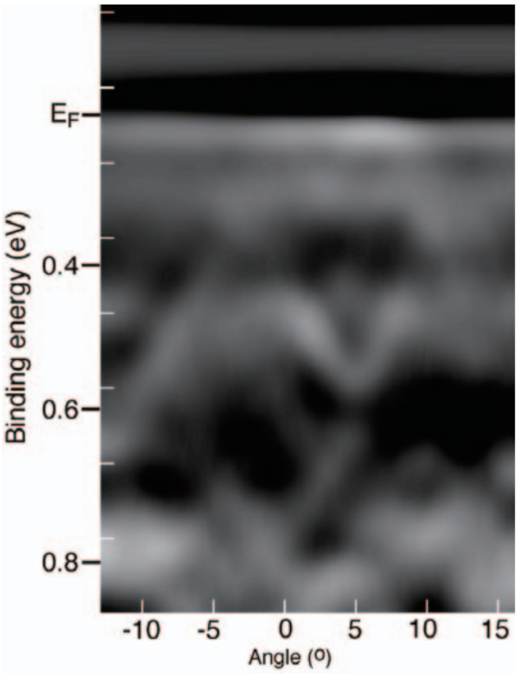

FIGURE 3. Second derivative of the ARPES spectra of CeRu$_2$Al$_{10}$ at $h\nu$ = 122 eV.

Figure 2 shows the high-resolution valence band spectra at 5.9, 10.5, and 18.3 K measured by laser light of $h\nu$ = 6.3582 eV. The spectra show a characteristic feature near the Fermi edge as shown in dotted line; suppression of the DOS starts around 30 meV. Recently detailed temperature dependence of the high-resolution spectra has been measured for CeT_2Al$_{10}$ (T = Ru, Os, and Fe) [4]. Our results reproduce well their results measured by Xe lamp light.

In Fig. 3 we show an example of the ARPES results of CeRu$_2$Al$_{10}$ measured at Ce 4*d*-4*f* resonant energy of $h\nu$ = 122 eV. We successfully measured angle-resolved spectra. We are still performing the measurements to obtain reliable data and to compare the DFT results.

References

1. V. M. T. Thiede, T. Ebel, and W. Jeitschko, *J. Mater. Chem.* **8**, 125 (1998).
2. T. Nishioka, Y. Kawamura, T. Takesaka, R. Kobayashi, H. Kato, M. Matsumura, K. Kodama, K. Matsubayashi, and Y. Uwatoko, *J. Phys. Soc. Jpn.* **78**, 123705 (2009).
3. Y. Zekko, Y. Yamamoto, H. Yamaoka, F. Tajima, T. Nishioka, F. Strigari, A. Severing, J.-F. Lin, N. Hiraoka, H. Ishii, K.-D. Tsuei, and J. Mizuki, Phys. Rev. B **89**, 125108 (2014).
4. T. Ishiga, T. Wakita, R. Yoshida, H. Okazaki, K. Tsubota, M. Sunagawa, K. Uenaka, K. Okada, H. Kumigashira, M. Oshima, K. Yutani, Y. Muro, T. Takabatake, Y. Muraoka, and T. Yokoya, J. Phys. Soc. Jpn. **83**, 094717 (2014).

XAFS analysis system with He-path at BL-3 and its performance

S. Yagi[1,2,3], C. Tsukada[2], S. Ogawa[2],G. Kutluk[3], H. Namatame[3], M. Taniguchi[3]

[1]*EcoTopia Science Institute, Nagoya University, Japan*
[2]*Graduate School of Engineering, Nagoya University, Japan*
[3]*Synchrotron Radiation Center, Hiroshima University, Japan*

Keywords: He-path, XAFS, Be window, liquid cell, SDD (silicon drift detector)

Electric conductivity is a key point, when we obtain a chemical state by some spectroscopic measurements. If the electric conductivity of materials is low or zero, such as semiconductors or insulators, the information related with the chemical state is not easily detected by the charge-up effect phenomenon. Especially, a spectrum measured by X-ray photoelectron spectroscopy (XPS) cannot be obtained or is distorted. Moreover, the charge-up effect by X-ray absorption fine structure (XAFS) with using soft X-rays under vacuum condition also cannot neglect. During XAFS measurements, some excited photoelectrons from the inner-shell are emitted to the vacuum level. When the photoelectrons return to the excited atoms or sample surface, the charge-up effect can be avoided. Therefore, one of the solutions is to fulfill the atmosphere of the sample to prevent the charge-up by inactive gas, such as He gas. From the above point of view, if we use soft-X-ray for the incident X-rays and detect the fluorescence X-rays under the inactive gas atmosphere, we can obtain XAFS spectrum of any kinds specimen. M. Nomura *et al.* [1, 2] and T. Akai [3] have reported the effectiveness of XAFS measurement system with He-path. In HiSOR facility at Hiroshima university, the He-path system is installed in the end station on BL-3[4]. This system is equipped Be-window with 20 μm thickness. The Be window can divide atmospheric pressure and ultra-high vacuum environment.

Usually, we use the fluorescence proportional counter (FPC) to detect the X-ray in BL-3. But the FPC has not good S/B ratio and energy resolution. In Aichi and Ritsumeikan synchrotron radiation centers (AichiSR and Ritsumeikan university SR), on the other hand, though both the operating electron energies are not large (1.2 GeV and 575 MeV), XAFS spectra are obtained with nice performance using the silicon drift detector (SDD). In this report, we will the recent years of He-path system for the XAFS measurement in BL-3 and performance.

FIGUREs 1a and 1b show photographic views of the end stations in BL-3 (HiSOR) and BL6N1 (AichiSR). Each system has the same Be window material.

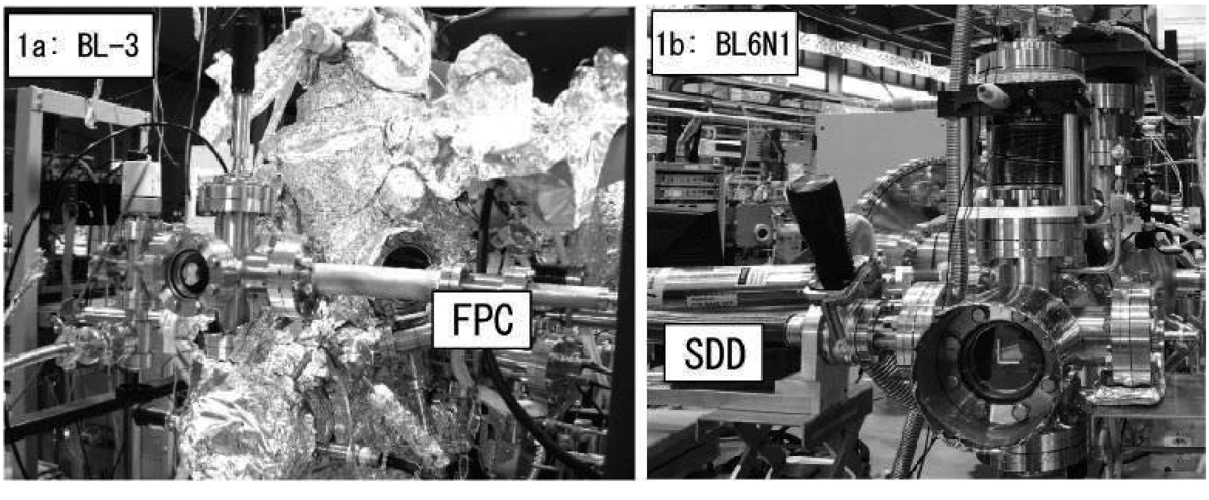

FIGURE 1a(left) and 1b(right): He-path systems in BL-3 and BL6N1.

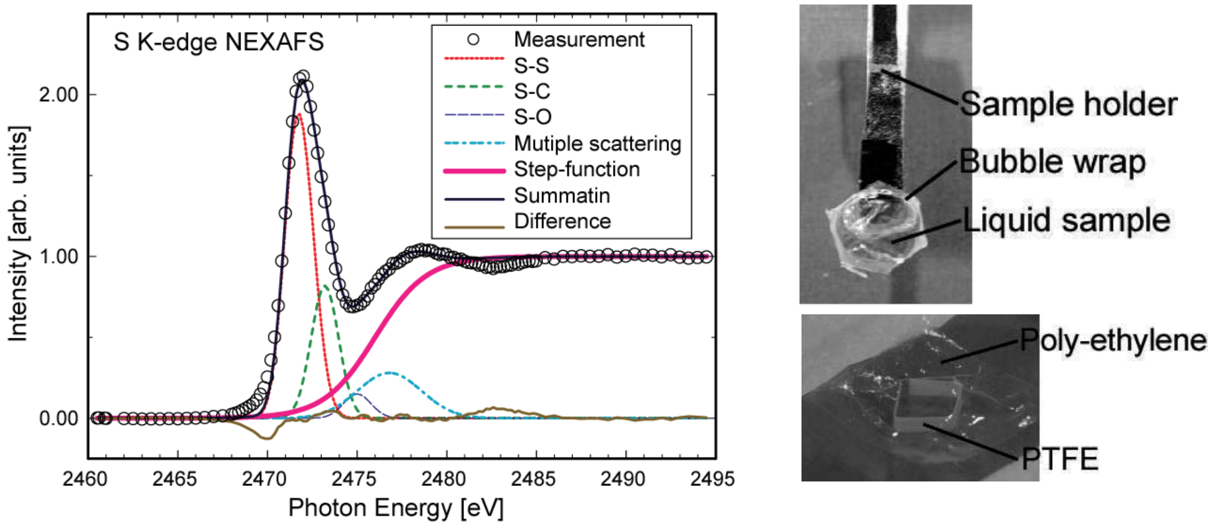

FIGURE 2a(left), 2b(right-up) and 2c(right-down): (2a) S K-edge NEXAFS spectrum for vulcanization reaction of squalene. (2b) bubble wrap cell for liquid sample. (2c) liquid sample made of poly-ethylene film and PTFE in AichiSR.

FIGUREs 2a, 2b and 2c show S K-edge NEXAFS spectrum and photographic views of liquid cells. The NEXAFS spectrum has been reported by Y. Menjo *et al.* in last HiSOR symposium [4]. The bubble wrap is made from poly-ethylene film with <20 μm thickness. Unfortunately, this bubble wrap includes a little amount of sulfur oxide as contamination. Thus, this liquid cell is unsuitableness for the S K-edge NEXAFS measurement of dilute sulfur materials. However, a hand-made liquid cell is using at BL6N1 in AichiSR [5]. This liquid cell is made of poly-ethylene film and poly-tetrafluoroethylene(PTFE) sheet and includes a very little amount of sulfur contamination in comparison with the bubble wrap.

FIGUREs 3a and 3b are MCA spectra at pre-edge (hν=2465 eV) and post-edge (hν=2490 eV), respectively. Those spectra have been measured in BL6N1 at AichiSR with SDD detector. The measured sample is compound composed of silicon, phosphorus and sulfur. Judging from these spectra, each fluorescence X-ray from silicon, phosphorus and sulfur elements is separated. If BL-3 has equipped the SDD, we think more performance of He-path XAFS system will be better.

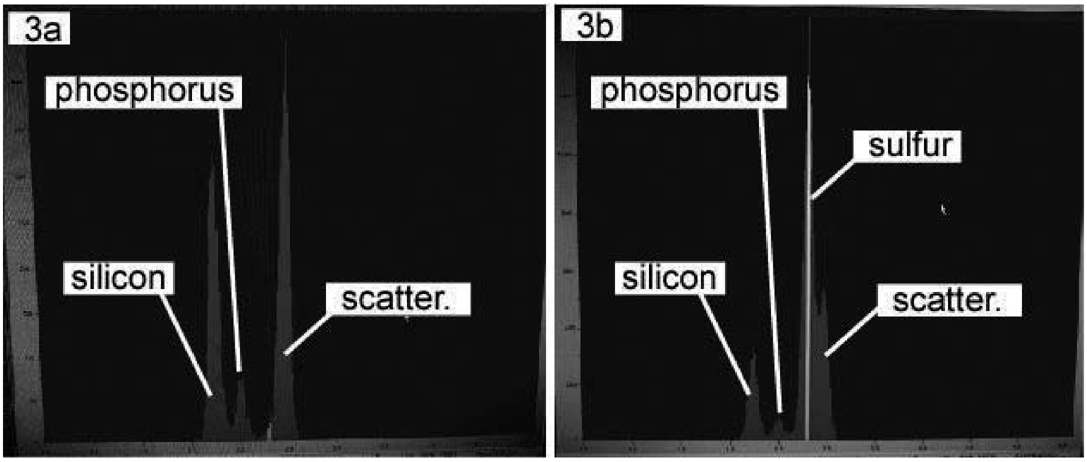

FIGURE 3. MCA spectra at (3a) pre-edge and (3b) post-edge, respectively.

REFERENCES

[1] M. Nomura and A. Koyama, J. Synchrotron Rad. **6,** 182 (1999).
[2] M. Nomura and A. Koyama, Nucl. Instrum. Methods Phys. Res., A467-468, 733 (2001).
[3] T. Akai, PHOTON FACTORY NEWS **20,** 32 (2003).
[4] Y. Menjo, G. Kutluk, T. Nomoto, T. Yoshida, S. Yagi, The 18th HiSOR symposium (2014).
[5] T. Nomoto and T. Murai, unpublished information.

Synchrotron light analyses for L-cysteine on the PC capped gold nanoparticle

C. Tsukada[a], T. Tsuji[a], K. Matsuo[b], T. Nomoto[c], T. Murai[c], G. Kutluk[b], H. Namatame[b], M. Taniguchi[b], T. Yaji[d], T. Ohta[d], S. Ogawa[a,c], T. Yoshida[c,e], S. Yagi[b,c,d,e]

[a]*Graduate School of Engineering, Nagoya University, Japan*
[b]*Hiroshima Synchrotron Radiation Center, Hiroshima University, Japan*
[c]*Aichi Synchrotron Radiation Center, Japan* [d]*The SR Center, Ritsumeikan University, Japan*
[e]*EcoTopia Science Institute, Nagoya University, Japan*

Keywords: Gold nanoparticle, Phosphatidylcholine, L-cysteine, NEXAFS, He-path system, Infrared spectroscopy

Gold nanoparticles (Au NPs) are taken notice of the uses of the hyperthermia for cancer cell [1] and the drug delivery system [2] in medical field. The Au NPs colloidal solution is generally fabricated by chemical reduction method. The fabrication method uses several reducing and dispersant agents. These agents have a possibility of low biocompatibility [3]. H. Takahashi *et al.* have reported that if the agents around Au NPs are replaced with phosphatidylcholine (PC) molecules, the biocompatibility of Au NPs becomes higher. To prepare the Au NPs with further higher biocompatibility, we focus on the solution plasma method reported by H. Nameki [4]. The solution plasma method uses three materials only, which are gold rods, electrolyte and distilled water. Thus, we decide to fabricate the Au NPs colloidal solution by using the solution plasma method and to cap the Au NPs surface by PC molecules. The PC molecule is constructed with the hydrophilic and the hydrophobic groups, as shown in FIGURE 1. In our previous study, we have proposed that the PC molecules adsorb on the Au sheet surface at the methyl group of N-CH_3 and the oxygen atoms of O-P, O=P, C-O and O=C bonds by carrying out nitrogen, oxygen and phosphorus K-edges near-edge X-ray absorption fine structure (NEXAFS) measurements [5]. Considering this result, we speculate that the PC molecules adsorb on the Au NPs surface at mainly the hydrophilic group. However, the behavior of the PC capped Au NPs is unknown. As one of purposes in this study, we investigate the behavior of the PC capped Au NPs by transmission electron microscopy (TEM) and infrared spectroscopy (IR) measurements. Subsequently, we assume that the PC capped Au NPs are injected in our body. Our body includes much amino acid molecules. L-cysteine is one of the amino acid molecules and has a thiol group (-SH). The thiol group reacts with easily metal surface compared to other functional groups. We have revealed the adsorption reaction under water/dry environments between the L-cysteine and the Au NPs fabricated by the solution plasma method by means of sulfur(S) K-edge NEXAFS measurement with He-path system [6]. The “dry environment” means the precipitate sample dried after adsorption reaction under water environment. The L-cysteine has adsorbed on rapidly the Au NPs surface at the thiol group, and dissociated into cysteine thiolate and atomic S. If the Au NPs are capped by PC molecules with high density, the L-cysteine has a possibility of not adsorbing on the PC capped Au NPs. As another of purpose in this study, we elucidate the adsorption reaction between the L-cysteine and the PC capped Au NPs under water/dry environments by means of S K-edge NEXAFS with He-path system.

The Au NPs colloidal solution was fabricated by the solution plasma method [4,6]. The potassium chloride powder was selected as electrolyte. The Au NPs colloidal solution in micro tube was cooled at 4°C. Subsequently, the PC powder (Egg, >99%) dissolved in milli-Q water at 4°C. The PC molecules aggregate easily in water environment. To remove the PC aggregations, the PC suspension was separated into the aggregations and the supernatant solution by performing centrifugation. The supernatant solution was added into the Au NPs colloidal solution cooled at 4°C, and the mixing solution was vortexed and kept at 4°C. The black colored precipitate, which was PC capped Au NPs, occurred after several hours. The precipitate was picked up to other micro tube and rinsed several times with the milli-Q water. The TEM sample of the precipitate was prepared by the negative staining method and was observed under the electron accelerating voltage of 100 kV by using H-7600 (Hitachi). IR sample was prepared by drying the precipitate or the PC suspension on Si wafer.

IR measurement was carried out at the SR center BL-15 in Ritsumeikan University. Subsequently, the L-cysteine powder was added into the precipitate under water environment. After promoting the adsorption reaction, the precipitate was rinsed several times with the milli-Q water. S K-edge NEXAFS measurement for the precipitate was carried out at HiSOR BL-3 and AichiSR BL6N1, respectively.

Taking account of the results of TEM observation and IR measurement, not shown here, we suppose that the PC caps around the Au NPs surface with high density by occurring the intermolecular force between the hydrocarbon chains of hydrophobic groups of PC molecules on Au NPs. FIGURE 2 shows S K-edge NEXAFS spectra for the PC capped Au NPs after reaction with the L-cysteine (a) under water environment and (b) under dry environment. The spectrum of L-cysteine aqueous solution is also shown as a standard. The spectra for (a) and (b) are normalized at approximately 2476 eV. The spectrum for the L-cysteine aqueous solution has a peak at 2472.6 eV assigned to σ*(S-C). The spectrum (a) "under water environment" has two peaks at 2473.1 eV and 2480.8 eV. We think that the peak at 2473.1 eV assigns σ*(S-C). The peak shift from 2472.6 eV to 2473.1 eV may indicate that the L-cysteine adsorbs on the Au NPs surface at thiol group and the S-H bond of L-cysteine dissociates [7]. The peak at 2480.8 eV shows the existence of SOx (x=2,3). We speculate that the SOx is formed by the coordination bond between H_2O and atomic S [6]. The atomic S may occur by dissociating of S-H and S-C bonds of the L-cysteine on Au NPs surface. On the other hand, the spectrum (b) "under dry environment" does not have the peak at 2480.8 eV. The shoulder at 2470 eV of the spectrum (b) appears dominantly compared to that of spectrum (a). The coordinated H_2O seems to desorb from atomic S on the Au NPs surface when the precipitate dries. We reveal that the PC capped Au NPs has the molecular adsorption site and the L-cysteine adsorbs on the Au NPs surface.

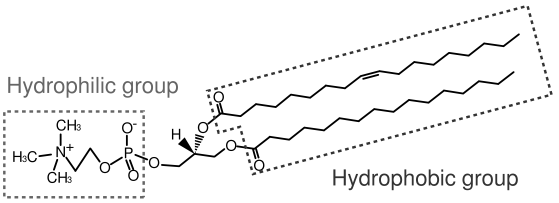

FIGURE 1. Structural formula of PC molecule.

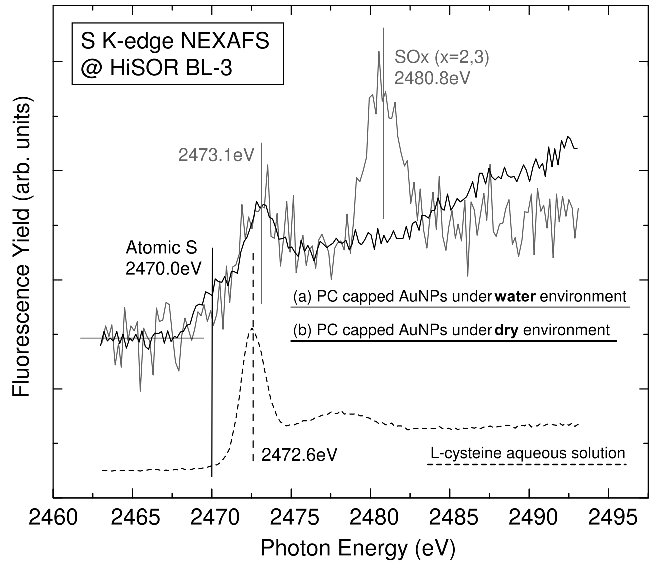

FIGURE 2. S K-edge NEXAFS spectra for the PC capped Au NPs after reaction with the L-cysteine (a) under water environment and (b) under dry environment. The spectrum of L-cysteine aqueous solution is also shown as a standard.

REFERENCES

1. H.-C. Huang, K. Rege, J.J. Heys, *ACS Nano* **4** (2010) 2892.
2. F. Wang, Y.-C. Wang, S. Dou, M.-H. Xiong, T.-M. Sun, J. Wang, *ACS Nano* **5** (2011) 3679.
3. E.E. Conner, J. Mwamuka, A. Gole, C.J. Murphy, M.D. Wyatt, *Small* **1** (2005) 325.
4. H. Nameki, *private communication in Aichi Prefectural Technical Report* (2010).
5. C. Tsukada, T. Tsuji, K. Matsuo, T. Nomoto, G. Kutluk, M. Sawada, S. Ogawa, T. Yoshida, S. Yagi, *IOP Conference Series: Materials Science and Engineering*, in press (2015).
6. C. Tsukada, T. Mizutani, S. Ogawa, T. Nomoto, Y. Abe, H. Nameki, K. Matsuo, G. Kutluk, S. Yagi, *e-Journal of Surface Science and Nanotechnology* **11** (2015) 18.
7. P. Zhang, T.K. Sham, *Physical Review Letters* **90** (2003) 245502-1.

Resonant Photoemission Studies of Electronic Ferroelectric $YbFe_2O_4$

T. Fukura[a], T. Wakita[a,b], A. Takeda[a], K. Terashima[a,b], K. Fujiwara[b], N. Ikeda[b],

Y. Muraoka[a,b], T. Yokoya[a,b]

[a] *Research Laboratory for Surface Science, Okayama 700-0011, Japan*
[b] *Graduate School of Natural Science and Technology, Okayama University, Okayama 700-0011, Japan*

Keywords: Electronic ferroelectricity, $YbFe_2O_4$, Resonant photoemission spectroscopy.

$YbFe_2O_4$ is a member of RFe_2O_4 (*R*: rare earths) family that is known as the mixed valence ferrites [1]. The ferroelectricity is considered to be driven by electron polarization between ordered Fe^{2+} and Fe^{3+}, different from the conventional ionic displactive-type ferroelectricity [2]. $YbFe_2O_4$ consists of alternating stack of Yb-O layers and double Fe-O layers in which Fe atoms form a triangular lattice. The average nominal valence state of Fe atoms is +2.5 in $YbFe_2O_4$, and an equal number of Fe^{2+} and Fe^{3+} coexist. Due to the frustration of the charge and spin originated from the triangle lattice, it exhibits sequential charge and spin order transitions as a function of temperature. To understand the physical properties, it is important to know the electronic structure directly involved in the transitions. However, there is no direct observation of the Fe 3*d* electronic states relevant to the transitions and hence electronic polarization.

In this study, we investigate the Fe 3*d*-derived states of $YbFe_2O_4$ using the resonant photoemission spectroscopy(RPES) across the Fe3*p* →3*d* photoabsorption threshold. The sample is high quality single crystal, as evidenced from the clear (1/3, 1/3, *l*) spots in single crystal XRD at room temperature, where *l* is integer and half-integer. The fresh surfaces were obtained with cleaving the samples under ultrahigh vacuum. In Figure 1, we show valence band spectra measured at photon energies of 53.2, 54.8, and 58.0 eV, normalized to the intensity at 4.5 eV binding energy. The photon energy of 53.2 eV is just below the Fe3*p*→3*d* photoabsorption threshold, that is, the spectrum is OFF resonance spectrum. The photon energies of 54.8 eV and 58.0 eV correspond to the structures of Fe^{2+} and Fe^{3+} in the XAS spectrum [3]. Therefore, the Fe^{2+} and Fe^{3+} derived states are expected to be enhanced with these photon energies (ON resonance spectrum). We found that, while intensity of the structure around 1.3 eV is enhanced with 54.8 eV photons, that around 3.5 eV is enhanced with 58.0 eV photons. These results indicate that Fe^{2+} and Fe^{3+} derived states are located at 1.3 eV and 3.5 eV, respectively. We will discuss the character of those states by comparing the resonance profile measured with constant initial state spectra of $YbFe_2O_4$ with those of other iron oxides [4].

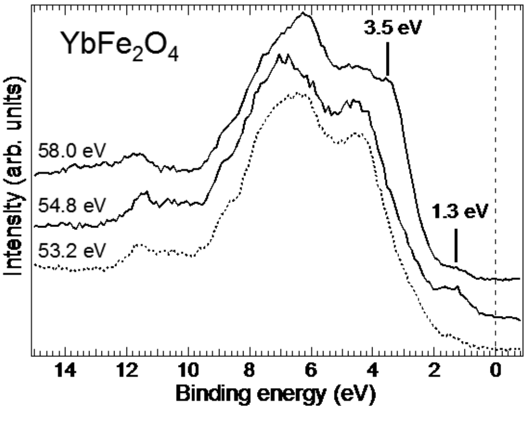

Figure 1. Resonant photoemission spectra of $YbFe_2O_4$

REFERENCES

1. N. Kimizuka et al., *Solid State. Commun.* 15, 1321 (1974).
2. N. Ikeda et al., *Nature(London)* 436, 1136 (2005).
3. Sara Lafuerza et al., *Phys. Rev. B* 90, 245137 (2014).
4. Robert J. Lad et al., *Phys. Rev. B* 39, 13478(1989).

14-B-3 BL-5

B 1*s*-2*p* Resonant Photoemission Studies of Heavily Boron-Doped Superconducting Diamond

A. Takeda[a], T. Wakita[a], T. Fukura[a], H. Okazaki[b], Y. Takano[b], S. Kurihara[c], H. Kawarada[c], T. Oguchi[d], Y. Muraoka[a], T. Yokoya[a]

[a]*Research Laboratory for Surface Science and Graduate School of Natural Science and Technology, Okayama University, Okayama 700-0011, Japan*
[b]*National Institute for Materials Science, Tsukuba, Ibaraki 305-0047, Japan*
[c]*Faculty of Science and Engineering, Waseda University, Shinjuku, Tokyo 169-8555, Japan*
[d]*Institute of Scientific and Industrial Research, Osaka University, Mihogaoka, Ibaraki, Osaka 567-0047, Japan*

Keywords: Diamond, X-ray absorption spectroscopy, Resonant photoemission spectroscopy

Diamond is famous jewel. Pure diamond is the hardest material, and has the highest thermal conductivity around room temperature. Electrically, diamond is a good insulator with a band gap of ~ 5.5 eV. In lightly boron-doped diamond, the physical properties are explained by impurity levels. In 2004, it was discovered that heavily boron-doped diamond exhibits superconductivity [1]. As two extreme cases, the metallic properties can be described by carriers in the impurity band formed by the impurity level [2], or in the host diamond band [3]. In the previous ARPES studies, we demonstrated that holes are introduced into the top of the diamond-like valence band in heavily boron-doped diamond [4]. On the other hand, role of the impurity band for the physical properties has been proposed theoretically [5], which should be clarified experimentally. In this study, we investigate the character of the states near the Fermi level with resonant photoemission spectroscopy (RPES), by which we can find what chemical role boron plays in the metallic state.

A heavily boron-doped single crystal (111) diamond film was homoepitaxially grown by microwave plasma assisted chemical vapor deposition (MPCVD) methods [6]. The transition temperature T_c was 10.2 K. As in Fig. 1, B *K*-edge X-ray absorption spectroscopy (XAS) spectrum for boron-doped diamond (111) film was obtained. Four features are observed, and marked with *a*, *b*, *c*, and *d*, consistent with previous XAS studies [7,8]. The features *c* and *d* are observed in the diamond conduction band [7]. The features *a* and *b* are identified to be in-gap states [8]. Comparison with B 1*s* core level PES allows us to assign that the feature *a* is related to metallic state [9]. Preliminary RPES results showed that resonance enhancement does not occur at narrow energy region near the Fermi level but occur over the whole valence band. We will discuss the implication of the results.

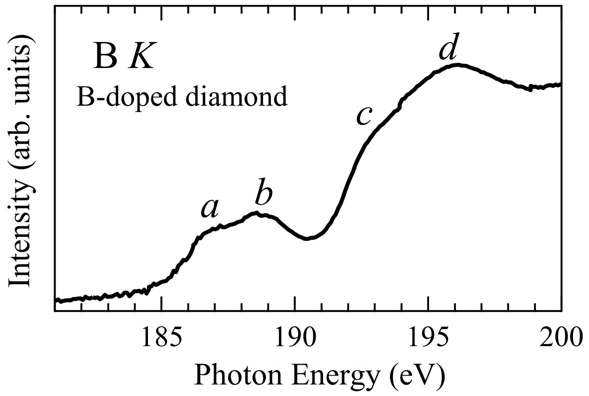

FIGURE 1. B *K*-edge X-ray absorption spectrum of boron -doped diamond. The four peaks are marked *a*, *b*, *c*, and *d*.

REFERENCES

1. E. A. Ekimov et al., *Nature* **428**, 542-545 (2004).
2. G. Baskaran et al., *J. Supercond. Nov. Magn*. **21**, 45-49 (2008).
3. L. Boeri et al., *Phys. Rev. Lett*. **93**, 237002 (2004).
4. T. Yokoya et al., *Nature* **438**, 647-650 (2005).
5. T. Shirakawa et al., *J. Phys. Soc. Jpn*. **76**, 014711 (2007); Y. Yanase et al., *ibid*. **78**, 034715 (2009).
6. H. Okazaki et al., *Appl. Phys. Lett*. (in press)
7. J. Iihara et al., *Jpn. J. Appl. Phys.* **44**, 6612-6617 (2005).
8. J. Nakamura et al., *J. Phys. Soc. Jpn*. **77**, 054711 (2008).
9. H. Okazaki et al., *J. Phys. Soc. Jpn*. **78**, 034703 (2009).

Doping dependent electronic properties of doped picene film

T. Hamada[a], T. Jabuchi[a], T. Wakita[a,b], Y. Muraoka[a,b], T. Yokoya[a,b]

[a] *Graduate School of Natural Science and Technology, Okayama University, Okayama 700-0011, Japan*

[b] *Research Laboratory for Surface Science, Okayama 700-0011, Japan*

Keywords: picene, superconductivity, photoemission spectroscopy

In 2010, it was found that the potassium(K)-doped picene solid shows superconducting critical temperatures of 7 and 18 K for K concentration (x) of around 3 [1]. K-doped picene is the first found superconductor in aromatic hydrocarbon. In contrast to the observation of superconductivity, the crystal structure and the K concentration of superconducting K-doped picene are not specified yet because of the significantly low shielding fraction and the unstableness under the atmospheric condition. In the theoretical study, the several optimized structures for K-doped picene solids are predicted and the band calculations for them shows that different ground states emerge depending on x ($x = 0, 2$: insulator, $x = 1, 3$: metal) [2].

To reveal the electronic structures of the K-doped picene solids experimentally, we have performed photoemission spectroscopy measurements for vacuum-evaporated K-doped picene films [3,4]. Such films have the advantage of ease to control potassium concentration and of less degradation of samples under the ultra-high vacuum condition. Figure 1 shows the valence-band spectrum from a K-doped picene film on a Au-coated stainless substrate measured with photon of 100 eV on the BL5 at HiSOR, together with a result of the molecular-orbital calculation for monoanion picene which convoluted with Gaussian (FWHM of 0.7 eV) to reproduce the observed spectrum [3]. The valence band spectrum of pristine picene (not shown) has no state at the Fermi level (E_F), while that of K-doped picene involves a new state near E_F. The observed K-doped spectrum is consistent with the one calculated including electron-phonon coupling, which clearly indicates the importance of the electron-phonon coupling in K-doped picene. Figure 2 shows the evolution of the valence band spectra of a picene film on a HOPG substrate upon K doping measured with Xe Iα [4]. They exhibit the appearance and the disappearance of Fermi edges depending on the potassium concentration, implying that the $K_x$picene film has multiple phases depending on x.

In this report, we will also preset some very recent results of the electrical resistivity measurements of vacuum-evaporated K-doped picene films.

REFERENCES

[1] R. Mitsuhashi*et al.*, Nature (London) **464**, 76 (2010).

[2] T. Kosugi*et al.*, Phys. Rev. B **84**, 214506 (2011).

[3] H. Okazaki *et al.*, Phys. Rev. B **82**, 195114 (2010).

[4] H. Okazaki *et al.*, Phys. Rev. B **88**, 245414 (2013).

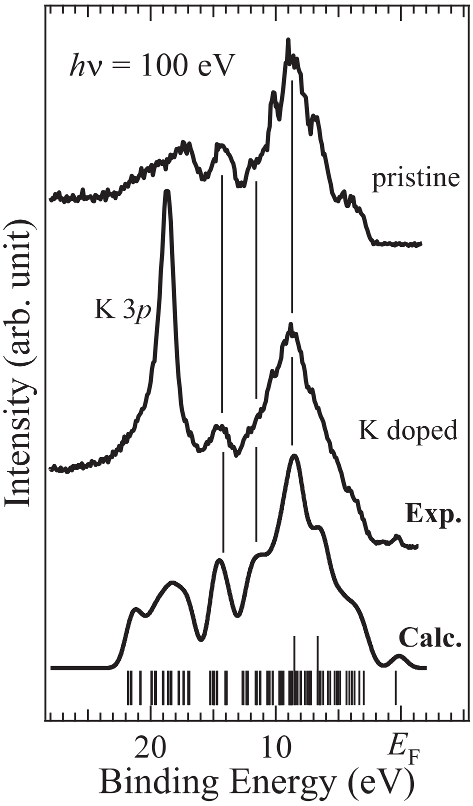

FIGURE. 1. Valence-band spectrum from K-doped picene film on a Au-coated stainless substrate using 100 eV photon energy, together with molecular-orbital calculation of monoanion picene with convoluted with Gaussian (FWHM of 0.7 eV) to reproduce the observed spectrum.

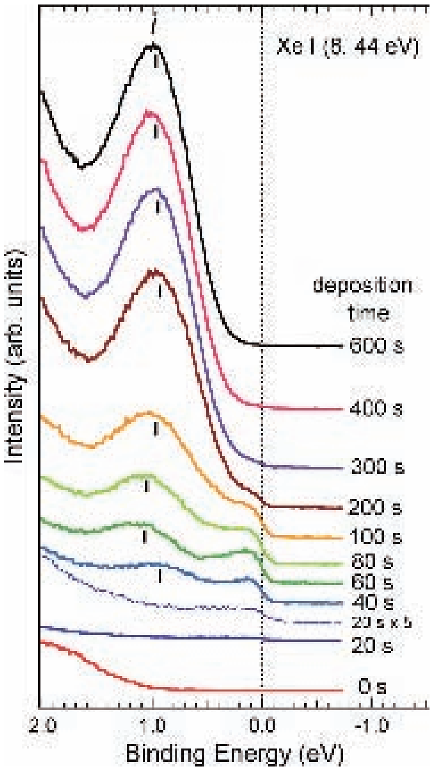

FIGURE. 2. Evolution of the valence band spectra of a picene film on a HOPG substrate upon K doping measured with Xe Iα.

Current activities of research and education on BL5

Y. Muraoka, T. Wakita, and T. Yokoya

Graduate School of Natural Science and Technology, Okayama University

Keywords: photoemission spectroscopy, photoelectron emission microscopy

Research and educational activities on beamline 5 (BL5) are presented. At BL5, we can perform angle-resolved photoemission spectroscopy (ARPES) and photoelectron emission microscopy (PEEM) measurements. The former can reveal the electronic and periodic structure of atomic scale for the sample surfaces. The latter can access topographical image contrast, elemental 2D contrast and their time evolution for the sample. Combing two measurements allow us to characterize phenomena, such as crystal growth on a surface, segregation, density fluctuation, adsorption phenomena related to catalysis and corrosion on a solid surface. Current researches we are doing are mainly, 1) study of the electronic structure of 1) aromatic molecules such as picene, 2) transition metal oxides such as VO_2 thin films which exhibits a first-order metal-to-insulator transition at 340 K and chromium dioxide CrO_2 thin films which are known as a half-metallic material, and new materials. We are also studying the chemical reaction between alkali metal ions like K^+ and Rb^+ and TiS_2 surface.

We use the BL5 for education activity, for example, practical education for undergraduate students at Okayama University. The students have an opportunity to study the synchrotron radiation mechanism of HiSOR and sometimes to experience XPS measurement which is very useful for the surface science research. Very recently, we have given a class of synchrotron radiation mechanism and XPS for students in Okayama university. We accepted about 20 students at various fields such as physics and biology in recent 3 years.

14-B-3 BL-5

Quantitative Estimation of Local Work Function by PEEM

T. Wakita, K. Terashima, Y. Muraoka, and T. Yokoya

The Graduate School of Natural Science and Technology, Okayama University, Okayama 700-8530, Japan,

Keywords: Photoelectron Emission Microscopy, Silicon, Silver, Film, Local Work Function

Controlling the arbitrary organization and array of atoms and molecules on a solid surface have been one of the main topics in course of rapid developments of nanotechnologies for a last few decades. A highlight in the early stage of these developments is the manipulation of *one atom* by using the scanning tunneling microscope [1]. Among such so-called “bottom-up” nanotechnologies, another fruitful approach is to utilize the surface reconstruction and the self-assembling of atoms and molecules on solid surfaces, in which whole atoms and/or molecules on the surfaces are arranged simultaneously. To construct more arbitrary and minute patterns in a wide area on a solid surface, full regulation of atomic diffusion on a solid surface will be needed. For this final goal, understanding of the diffusion process of certain amount of atoms (but not whole atoms) on a surface is important. Actually, several studies on the diffusion process of micro-size films have been reported so far, and photoelectron emission microscopy (PEEM) has been used in a few of them, mainly because of the ability of the real-time observation when it is used with a sufficiently bright light source, e.g. Hg lamp [2-5]. The PEEM image measured with a Hg lamp provides a 2D lateral distribution of the relative values of the local work function on a solid surface. The thermal diffusive motions of atoms are closely related with the variation of the local work function. However, a general method to estimate quantitatively the local work function from PEEM images is not known yet. In this study, we found that there is a possibility to estimate the local work function quantitatively from the intensity variation of PEEM images in the temperature-decreasing process.

We have investigated the diffusion process of Ag films of micro-size (“Ag micro-films”) on Si surfaces by using photoelectron emission microscopy (PEEM) with synchrotron radiation (SR). The measurements were performed on the BL5 (the Okayama University beamline) at HiSOR. The experimental station is equipped with PEEM III (Elmitec GmbH). The spatial resolution is about 30 nm when a mercury lamp is used as an illumination source and it is better than 1 μm with SR. Commercial *p*-type Si(100) wafers (boron doped) were used as sample substrates. Clean Si(100)2x1 surfaces were prepared by heating the samples up to 1520 K for 5 s with electron bombardment and clear 2x1 diffraction patterns were observed by low energy electron diffraction (LEED). Ag micro-films (7 ML) were evaporated on the Si surfaces from a heated tungsten (W) filament on which two Ag droplets with a rate of 1.2 Å/min through a *circular* pin-hole (the diameters is 30 μm) at room temperature. The two-dimensional (2D) contours of the PEEM image of Ag micro-films shown in figure 1 clearly exhibit the good correspondence with those of Ag droplets. This image is measured with Hg lamp and the field of view is 150 μm. The measuring time is 5 sec. There is a relatively large difference between the work function of a Ag surface (4.28 eV) and that of a Si(100)2x1 surface (4.9 eV). It is therefore considered that the image with Hg lamp corresponds to the Ag distribution on this surface, and we confirmed it from PEEM measurements with SR light around the Si $L_{2,3}$-edge (not shown).

We observes a surface diffusion process for this sample during a rise in sample temperature from room temperature to 500 ℃ as shown in figure 2(a). Figure 2(b) shows the snap shots of the time-evolution of 3D-plotted PEEM images. There is a relatively small change until about 200 ℃ and the changes are promoted in the temperature range between 200 and 500 ℃. We plot the intensity variations as a function of the temperature at position on the Si substrate (the open square in the PEEM image) as a gray curve in figure 3. It shows that the intensity variation has three temperature ranges: first, it shows a relatively small increase until around 200 ℃ (range 1), and decreases largely between about 200 and 440 ℃ (range 2), and then rapidly increases over about 440 ℃ (range 3). Moreover, from a careful beholding of the motion of the intensity around Ag films in each range, we found that, in range 1 and 3, the intensity expands from the film to Si substrate, although the intensity moves toward the film in range 2. Since the PEEM image measured with Hg lamp just exhibits a 2D lateral distribution of the local work function of the surface as mentioned above, one should carefully examine whether these intensity motions are able to be directly interpreted as the motion of Ag atoms. For a further argument, it is necessary for us to establish a method to estimate the real motion of Ag atoms from the variation of the local work function, and then we focus on the intensity variation in the temperature-decreasing process (the black curve in figure 3). It shows a monotonic decrease and it is considered that this intensity variation in the temperature-decreasing process depends practically only on the sample temperature, especially in the lower temperature range. If the variation in the thermal electron emission from the sample surface is the main origin of this intensity variation, the black curve in figure 3 should be reproduced by the Richardson-Dushman formula which includes a local work function as a parameter. The dashed curve in figure 3 is a fitting result. This fitting, however, results in an unphysical value of the local work function. We will discuss the reason and the method to obtain a physically reasonable value for the local work function.

REFERENCES

1. D. M. Eigler and E. K. Schwaizer, *Nature (London)* **344**, 524-526 (1990).
2. D. Reuter et al., *Phys. Rev. B* **57**, 2520 (1998).
3. K. R. Rose et al., *Phys. Rev. Lett.* **100**, 016103 (2008).
4. H. Yasuaga and S. Yoda, *Jpn. J. Appl. Phys.* **30**, 1822 (1991).
5. F. X. Shi et al., *Surf. Sci.* **493**, 331 (2001).

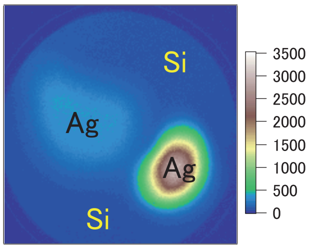

FIGURE 1. PEEM image of two Ag-micro films on a Si(100)2x1 surface. The field of view is 150 μ m.

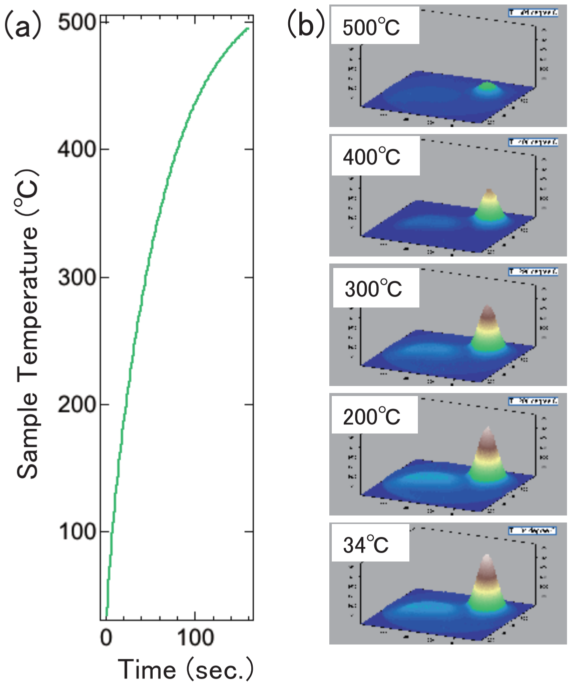

FIGURE 2. (a) Sample temperature as a function of time. (b) Snap shots of the evolution of 3D-plotted PEEM images of the sample when the temperature increases.

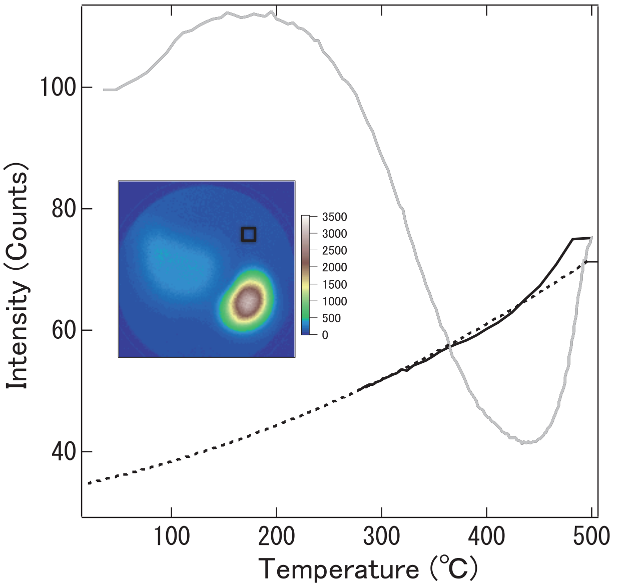

FIGURE 3. Intensity variations as a function of temperature at position on the Si substrate (the open square in the PEEM image). The gray curve shows the intensity variation in the temperature-increasing process, and the black curve the one in the temperature-decreasing process, respectively. The dashed curve is a fitting result obtained by using Richardson-Dushman formula.

Photoelectron spectroscopy study of $(Na_{1-x}Ca_x)Cr_2O_4$

H. Yamaoka[a], Y. Yamamoto[b], M. Nakatake[c], Y. Sakurai[d], N. Tsujii[d], K. Shimada[c], H. Namatame[c], M. Taniguchi[c,e], and J. Mizuki[b]

[a]*RIKEN SPring-8 Center, Sayo, Hyogo 679-5148, Japan*
[b]*Graduate School of Science and Technology, Kwansei Gakuin University, Sanda, Hyogo 669-1337, Japan*
[c]*Hiroshima Synchrotron Radiation Center, Hiroshima University, Higashi-Hiroshima, Hiroshima 739-0046, Japan*
[d]*Quantum Beam Center, National Institute for Materials Science, 1-2-1 Sengen, Tsukuba 305-0047, Japan*
[e]*Graduate School of Science, Hiroshima University, Higashi-Hiroshima, Hiroshima 739-0046, Japan*

Keywords: electronic structure, photoelectron spectroscopy, $NaCr_2O_4$, metal insulator transition

$NaCr_2O_4$ was recently discovered by a high-pressure synthesis to occur in calcium ferrite type structure, where one dimensional electronic correlations and geometrical frustrations can coexist [1-5]. It shows unconventional colossal magnetoresistance (CMR) below antiferromagnetic ordering temperature of T_N = 125 K. The CMR effect in $NaCr_2O_4$ is progressively enhanced with decreasing temperature with no thermal or field hysteresis. CMR is often observed in ferromagnetic manganese oxide, but not in chromium oxide so far. CMR is observed not only in the vicinity of the magnetic phase transition, but also rather more prominent with decreasing temperature. The conventional CMR effect appears only around ferromagnetic transition temperature and it is originated by the suppression of thermal fluctuation of the ferromagnetic moment by magnetic field. Therefore CMR normally becomes smaller with decreasing temperature and the resistivity is significantly low at low temperatures even without magnetic field. Thus the temperature dependence of CMR of $NaCr_2O_4$ is anomalous.

In $NaCr_2O_4$ recent x-ray absorption spectroscopy study at O *K*-edge shows the holes on the oxygen ions, indicating a negative charge transfer energy. NMR for $NaCr_2O_4$ showed the mixed valence state of $Cr^{3.5+}$ [2].Ca-substitution to the Na site changes the Cr valence from 3.5 for $NaCr_2O_4$ to 3 for $CaCr_2O_4$. In $Na_{1-x}Ca_xCr_2O_4$ Néel temperature T_N rapidly decreases with decrease of Na content [5]. Spin glass behavior has been observed for $0.4 < x < 0.9$. Thus in many aspects $NaCr_2O_4$ shows very different physical properties compared to other 3*d* oxide compounds and is rather similar to the classical Mott-Hubbard metal-insulator transition of V_2O_3, which is characterized with $U_{dd} < \Delta$, where U_{dd} and Δ are onsite *d-d* Coulomb repulsion energy and charge transfer energy determining the band gap, respectively.

The electronic structure may play an important role for above unusual physical properties, but no measurement has been reported so far. We have been making photoelectron spectroscopy (PES) study for $NaCr_2O_4$. Here we extend our PES study to Ca-substituted systems of $(Na_{1-x}Ca_x)Cr_2O_4$. $(Na_{1-x}Ca_x)Cr_2O_4$ were synthesized using a high pressure and high temperature technique [1].

Figure 1 shows the *x*-dependences of the valence band spectra and Na 2*p* and Ca 3*p* spectra. The intensity is normalized by the area. The valence band mainly consists of Cr 3*d* just below the Fermi level and O 2*p* as shown in Fig. 1(a). We observe increase of the Cr 3*d* peak intensity with the Ca substitution. The Ca-substitution also causes the decrease of the 3*d* DOS at the Fermi edge because the system is close to insulator with *x* as shown in Fig.

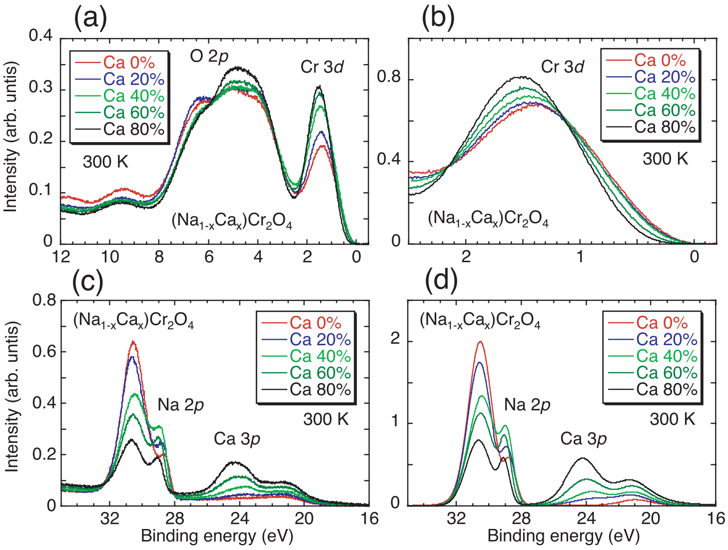

FIGURE 1. *X*-dependence of the valence band and core-level (Na 2*p* and Ca 3*p*) spectra of $(Na_{1-x}Ca_x)Cr_2O_4$at 300 K and *h*ν = 85 eV.

1(b) (expanded view of the valence band spectra near the Fermi edge). Figure 1(c) shows Na 2*p* and Ca 3*p* core-level spectra. In Fig. 2(d) we show the spectra where background in Fig. 1(c) is subtracted. Na 2*p* peak is considered to have surface and bulk contribution, forming double peak structure [6]. It is noted that Na 2*p* spectra should have spin-orbit separated peaks, but the peak separation is the order of 0.2 eV, which is much smaller than the peak separation in Fig. 2(c). We observe the shift of the Ca 3*p* peak to lower binding energy with increase of Ca content.

Figure 2 shows the temperature dependence of the valence band and core-level (Na 2*p* and Ca 3*p*) spectra. Weak temperature dependence is observed in the temperature range measured.

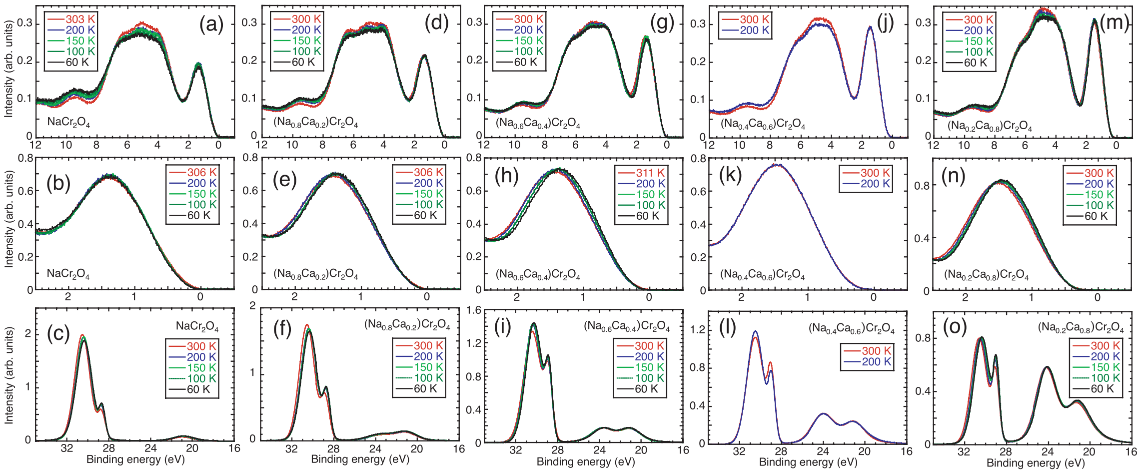

FIGURE 2. Temperature dependence of the valence band and core-level (Na 2*p* and Ca 3*p*) spectra of (Na$_{1-x}$Ca$_x$)Cr$_2$O$_4$ at *h*ν = 85 eV.

References

1. H. Sakurai, T. Kolodiazhnyi, Y. Michiue, E. takayama-Muromachi, Y. Tanabe, and H. Kikuchi, Angew. Chem. Int. Edit. **51**, 6653 (2012).
2. H. Takeda, M. Itoh and H. Sakurai, Phys. Rev. B **86**, 174405 (2012).
3. H. Takeda, Y. Shimizu, M. Itoh, H. Sakurai, and E. Muromachi, J. Korean Phys. Soc. **62**, 1914 (2013).
4. H. Sakurai, J. Korean Phys. Soc. **63**, 583 (2013).
5. H. Sakurai, Phys. Rev. B **89**, 024416 (2014).
6. D. M. Riffe, G, K. Wertheim, and P. H. Citrin, Phys. Rev. Lett. **67**, 116 (1991).

14-B-12 BL-7

Angle-Resolved Photoemission Spectroscopy in topological insulator SnTe thin films

Ryota Akiyama[a,b], Kazuki Fujisawa[a], Tomonari Yamaguchi[a], Ryutaro Sakurai[a],
Shinji Kuroda[a], Masashi Nakatake[c], and Akio Kimura[d]

[a]Department of Material Sciences, University of Tsukuba, 1-1-1 Tennoudai, Tsukuba, Ibaraki, Japan
[b]Department of Physics, The University of Tokyo, 7-3-1 Hongo, Bunkyo-ku, Tokyo, Japan
[c]Hiroshima Synchrotron Radiation Center, Hiroshima University, 2-313 Kagamiyama, Higashi-Hiroshima, Hiroshima, Japan
[d]Graduate School of Science, Hiroshima University, 1-3-1 Kagamiyama, Higashi Hiroshima, Hiroshima, Japan

Keywords: topological insulator, topological crystalline insulator, spin orbit interaction, weak antilocalization

Topological insulator (TI) is a new class of materials. TI attracts attention much recently because of the novel functionality and the possibility for application. The surface state (SS) of TIs has a Dirac-cone-like band structure where the spin of carriers is locked with their momentum except for $k = 0$. The SS of TIs is metallic protected by time-reversal symmetry and exceedingly high mobility is expected in the transport of mass-less Dirac fermions in the SS. Recent investigations have paved the way for a new type of TIs, that is, topological crystalline insulators (TCIs), in which the topological SS is protected by the crystal mirror symmetry, instead of the time-reversal symmetry. SnTe was predicted to be one of the TCIs whose SS is protected by mirror symmetry with respect to the {111}, {001}, and {110} of the rock-salt crystal structure[1,2].

In this study, we aimed to observe the topological SS in thin films of SnTe by angle-resolved photoemission spectroscopy (ARPES). Topological SS of SnTe have been investigated in the bulk samples. Thin films are useful to decrease the contribution by the bulk part in the electrical transport measurements. However, since fabrication of the high quality thin film is difficult, the ARPES measurements in SnTe thin films have not been reported enough so far.

Since the crystal mirror symmetry protects the topological SS in TCIs, breaking of the time-reversal symmetry should not open the gap. This point is quite different from the property of TIs. The unopened gap in TCIs means that the mass-less Dirac Fermion can exists even near the Dirac point. Whether the gap opens or not has been checked by doping a magnetic atom into TIs. The robustness to breaking of the time-reversal symmetry in TCIs is not understood totally until now. Then, we doped Mn into SnTe, and checked the surface band dispersion by ARPES with optimized samples by molecular beam epitaxy (MBE) equipment. In parallel with such measurements, the electrical transport measurements were done with PPMS (Quantum Design) from the room temperature to low temperature, and external magnetic field dependence of the transport were observed.

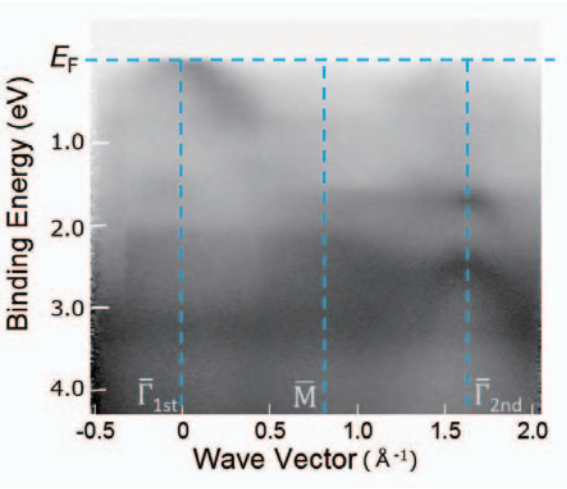

FIGURE 1. The ARPES image of the (Sn,Mn)Te thin film with the incident photon energy of 60 eV.

The (111) oriented (Sn,Mn)Te thin film was grown on $BaF_2(111)$ substrate at the temperature of 230°C after the thermal cleaning at 330°C for 1 hour in the growth chamber. The k-cell of Sn, Te, and Mn were used for the growth. The Sn and Te beam flux ratio is 1:3(Te-rich condition). The Mn beam flux was set to Sn:Mn = 100:0.57. The atom ratio of Mn to Sn and Mn, estimated by Electron Probe MicroAnalyser (EPMA), is 0.52%. The thickness is 112 nm. The surface of grown thin films needs to be clean and abrupt. The resolution and intensity of ARPES strongly depend on the quality of surface of the crystal. Therefore, the protection of the surface after the growth is very important for ARPES measurements. Then, we adopted the Te cap as a protection layer on the (Sn,Mn)Te surface. The Te cap was removed by heating the films in the ultra high vacuum environment in the preparation chamber of ARPES around 220°C.

The observed ARPES (Sn,Mn)Te thin film at 5 K is shown in Fig. 1. The incident photon energy is 60 eV. The Fermi level crosses the valence band of (Sn,Mn)Te because the carrier concentration measured by the Hall measurement is quite high ($\sim 10^{21}$cm^{-3}) due to many Sn vacancies. The previous reported ARPES images in the bulk sample of SnTe show the similar ARPES image of the degenerate semiconductor. This suggests that the feature of the whole band structure is preserved even when Mn atoms are doped into the thin film with low concentration. The Dirac-cone is predicted to appear at $\overline{\Gamma}$ and $\overline{\mathrm{M}}$ points[3]. However, from our results we can not separate the surface state denoted by the Dirac-cone from the valence band definitely because the Fermi level lies in the valence band. Therefore, we investigated also the surface state by electrical transport measurements. The system having the strong spin-orbit interaction, the weak antilocalizaiton(WAL) can occur. The two electrons scattering along the closed path destructive interfere, and therefore the backscattering is prohibited. The resistance under the zero magnetic field is lower than that under the non-zero magnetic field because of the suppression of the backscattering.

In TIs or TCIs, the quantum interference occurring in the WAL is different mechanism from the spin-orbit interaction system. The origin of the quantum interference is π Berry phase shift. Fig. 2 shows the longitudinal magnetoresistance (extracted symmetric component) at the temperature range of 4 - 30 K. The WAL curve was observed at 4 K, and it nearly disappears at $T > 6$ K. The curve at 4 K was fitted by the Hikami-Larkin-Nagaoka equation as follows[4],

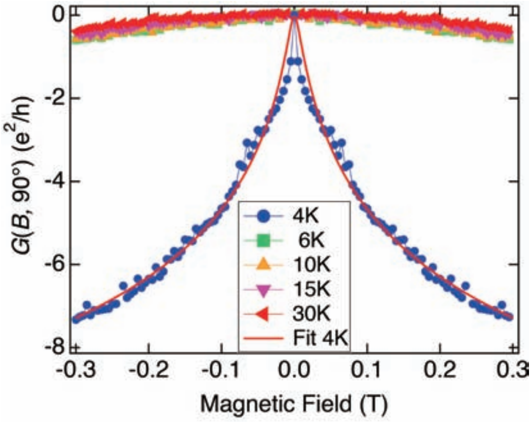

FIGURE 2. The dots represent WAL at the temperature of 4 – 30 K. The red curve represents fitting result by the Hikami-Larkin-Nagaoka equation.

$$\sigma_{2D} \equiv \sigma_{2D}(B) - \sigma_{2D}(0) = -\frac{\alpha e^2}{2\pi\hbar^2}\left[\ln\left(\frac{\hbar}{4Bel_\phi^2}\right) - \psi\left(\frac{1}{2} + \frac{\hbar}{4Bel_\phi^2}\right)\right]. \qquad (1)$$

The fitting parameters of α and $l_\phi$are the coefficients related with the number of the path, and the electrons' coherent length, respectively. According to the results of the fitting, α and l_ϕ = -2.49, 261 nm. The value of α indicates theoretically 1 path per -0.5. Therefore, 8 paths and α = 4 is predicted in the SnTe(111) surface considering the Dirac-cones on the TSS. However, α = -2.49 in this sample indicates that there are couples of transport channels among the surface channels or between the surface channels and the bulk channels. The abrupt disappearance of the WAL at $T > 6$ K indicates that the coherence factor such as phonon scattering is relatively strong in this sample. The phase coherent length, 261 nm, is comparable with the previous reports [5]. The carrier concentration was estimated to be 6.9×10^{21} cm^{-3} by the Van der Pauw method at 4 K. This indicates that the Fermi level lies in the valence band, and this sample is the degenerate semiconductor. Thus, the bulk contribution in the electrical transport is large in this sample.

From the observation of the WAL, the TSS is protected by the mirror symmetry for the Mn concentration up to at least 0.52% although the time-reversal symmetry breaks due to doping of Mn atoms. This suggests that unless the mirror symmetry breaks by doping magnetic atoms the TSS can be protected even with breaking the time-reversal symmetry.

These results help to understand the protection of the TSS in TCIs, which remains veiled even now. More intense research is required to clarify the effect of the mirror symmetry and the time-reversal symmetry on TCIs systematically.

REFERENCES

1. T. H. Hsieh, H. Lin, J. Liu, W. Duan, A. Bansil, and L. Fu, Nat. Commun. **3**, 982 (2012).
2. L. Fu, Phys.Rev.Lett. **106**, 106802 (2012).
3. Y. Tanaka, T. Shoman, K. Nakayama, S. Souma, T. Sato, T. Takahashi, M. Novak, K. Segawa, and Y. Ando, Phys. Rev. B **88**, 235126 (2013).
4. S. Hikami, A. Larkin, and Y. Nagaoka, Prog. Theor. Phys. **63**, 707 (1980).
5. B. A. Assaf, F. Katmis, P. Wei, B. Satpati, Z. Zhang, S. P. Bennett, V. G. Harris, J. S. Moodera, and D. Heiman, Appl. Phys. Lett. **105**, 102108 (2014).

14-A-6, 7 BL-7, RIPES

Valence- and Conduction-Band Electronic Structures of $Pd_{40}Cu_{20}Ge_{40}$ Metallic Glass Having a Curious Structural and Thermodynamic Properties

Shinya Hosokawa[a], Tokujiro Yamamoto[b], Hidemi Kato[c], Masasi Nakatake[d], and Hitoshi Sato[d]

[a] *Department of Physics, Graduate School of Science and Technology, Kumamoto University, Kumamoto 860-8555*

[b] *Department of Mechanical and Intelligent Engineering, Graduate School of Engineering, Utsunomiya University, Utsunomiya 321-8585*

[e] *Institute for Materials Research, Tohoku University, Sendai 980-8577*

[d] *Hiroshima Synchrotron Radiation Center, Hiroshima University, Higashi-Hiroshima, 739-0046*

Keywords: Metallic glass, Core-level photoemission spectroscopy, Valence band density of states

The ratio of glass transition- and melting temperatures, T_g/T_m, is widely employed as a simple index to characterize a glass-forming ability of glasses [1]. Generally, values of 3/2 or at smallest 1/2 were observed in various types of glasses, such as oxide, organic, and metallic glasses. Exceptions were only observed in simple polymer glasses, such as polyethylene (0.35) and polytetrafluoroethylene (0.26). Recently, Yamamoto et al. [2] have found a curious metallic glass, $Pd_{40}Cu_{20}Ge_{40}$, having a very low T_g and an extremely small T_g/T_m of 0.36, where T_g = 52°C and T_m = 625°C. Surprisingly, this metallic glass is formable even in hot water like polymer glasses.

To clarify an origin of such a small T_g/T_m value in the $Pd_{40}Cu_{20}Ge_{40}$ metallic glass from a partial structural point of view, anomalous x-ray scattering (AXS) experiments were performed close to the Pd, Cu, and Ge *K* x-ray absorption edges, and the obtained differential data were analyzed using reverse Monte Carlo modeling [3,4]. As a result, a structural hierarchy was realized, i.e., covalently bonded $GePd_4$ clusters and Cu atoms with metallic bonding between the clusters. In this study, we have investigated a formation of the $GePd_4$ covalent clusters from a viewpoint of electronic structures using photoemission and inverse-photoemission spectroscopy (PES and IPES).

A $Pd_{40}Cu_{20}Ge_{40}$ metallic glass sample was manufactured at Institute for Materials Research, Tohoku University by a normal melt-spinning technique with a tapered silica nozzle. The glass phase of the obtained ribbons was examined by x-ray diffraction and transmission electron microscopy. The composition of the sample was confirmed to be nominal value by an electron-probe micro-analysis equipment.

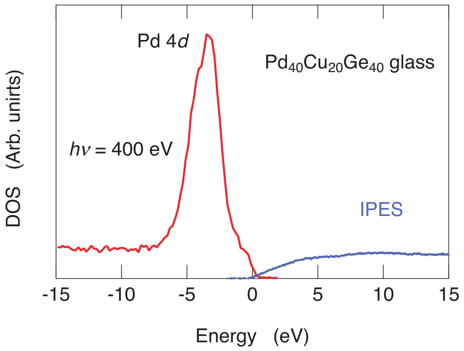

FIGURE 1. PES and IPES spectra of $Pd_{40}Cu_{20}Ge_{40}$ metallic glass.

The PES measurements were carried out using high-resolution PES spectrometer installed at BL-7 of HiSOR. The measurements were performed in the incident photon energy range of 30-400 eV to obtain valence-band density of states (DOS). We also measured core-level PES spectra for Pd 3*d* (-340 eV), Cu 3*p* (-76 eV), and Ge 3*d* (-28 eV) levels to examine the chemical states around each constituent element. The IPES spectra were also obtained using the RIPES spectrometer at HiSOR to measure the conduction-band DOS.

Figure 1 shows the valence- and conduction-band DOS obtained from PES and IPES measurements, respectively. In the valence band, a sharp peak at about -4 eV is seen together with a shoulder at about -4.5 eV, both of which originate from Pd 4*d* electrons. The energy position of these structures is larger in binding energy than those of pure Pd polycrystalline metal, $Pd_{40}Ni_{40}P_{20}$, and $Pd_{42.5}Ni_{7.5}Cu_{30}P_{20}$ bulk metallic glasses [5]. Also, the magnitude of DOS near the Fermi energy is very small and comparable with that in $Pd_{42.5}Ni_{7.5}Cu_{30}P_{20}$ bulk metallic glasses [5]. Since the incident photon energy dependence of the PES measurements enables one to estimate the element- and orbital angular momentum-selective DOS information, partial DOS could be estimated and will be given elsewhere.

Figures 2(a) and (b) show core-level PES spectra of the $Pd_{40}Cu_{20}Ge_{40}$ metallic glass for the (a) Pd 3*d* and (b) Ge 3*d* levels respectively. The Pd $3d_{5/2}$ core level is located at about -336.5 eV as a sharp peak, which is deeper in binding energy than those of $Pd_{40}Ni_{40}P_{20}$, $Pd_{40}Cu_{40}P_{20}$, and $Pd_{42.5}Ni_{7.5}Cu_{30}P_{20}$ bulk metallic glasses [6]. From these results, Pd has a single chemical state, and the electrons are located in a stable state, such as in a partially covalent bonding state.

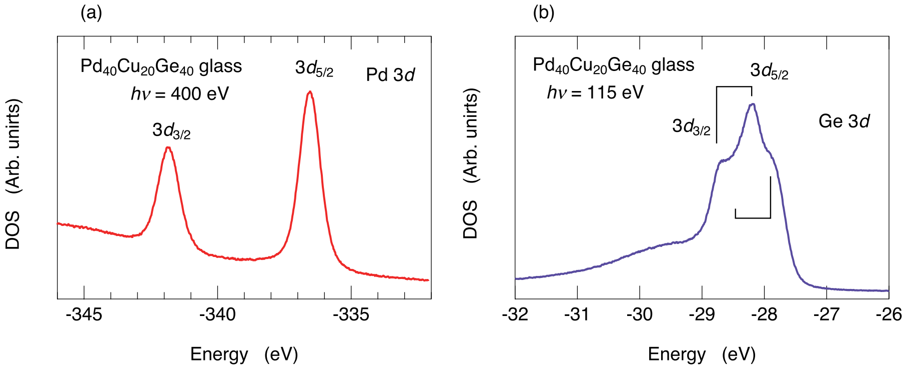

FIGURE 2. Core-level PES spectra of $Pd_{40}Cu_{20}Ge_{40}$ metallic glass for (a) Pd 3*d* and (b) Ge 3*d* levels.

The Ge 3*d* level should be double peaks of $3d_{3/2}$ and $3d_{5/2}$ with a difference of 0.6 eV. However, the spectra are composed of a peak at about -28.2 eV with shoulders at the both sides of the peak. Therefore, at least two core-level pairs are contributed to form the Ge 3*d* spectra as indicated by solid lines, and mainly two different chemical states are expected for the Ge atoms. As mentioned above, the AXS data showed the existence of $GePd_4$ covalent clusters, while another atomic state of metallic bonding is also possible for the Ge atoms. The present core-level PES result would be a proof for the coexistence of these covalent and metallic bonding states in the Ge atomic sites. For the further discussion, it is necessary to analyze the obtained PES and IPES data carefully by a curve-fit analysis, which is now in progress.

This work was performed under the inter-university cooperative research program of the Institute for Materials Research, Tohoku University (Project No. 14K0033).

REFERENCES

1. A. Inoue, *Acta Mater.* **48**, 279 (2000).
2. T. Yamamoto et al., *J. Non-Cryst. Solids* **359**, 46 (2013).
3. T. Yamamoto et al., *J. Phys.: Conf. Ser.* **519**, 012005 (2014).
4. S. Hosokawa, *Mater. Sci. Forum* **783-786**, 1907 (2014).
5. S. Hosokawa, *Acta Mater.* **55**, 3413 (2007).
6. S. Hosokawa, *Phys. Rev. B* **80**, 174204 (2009).

Electronic structure of mineral tetrahedrite $Cu_{12}Sb_4S_{13}$ and $Cu_{10}Zn_2Sb_4S_{13}$ studied by photoemission and inverse-photoemission spectroscopies

T. Nagasaki[a], A. Rousuli[b], H. Sato[c], M. Nakatake[c], G. Kutluk[c], K. Suekuni[d], H. Tanaka[d], T. Takabatake[d], H. Namatame[c] and M. Taniguchi[b,c]

[a]*Faculty of Science, Hiroshima University, Higashi-Hiroshima 739-8526, Japan*
[b]*Graduate School of Science, Hiroshima University, Higashi-Hiroshima 739-8526, Japan*
[c]*Hiroshima Synchrotron Radiation Center, Hiroshima University, Higashi-Hiroshima 739-0046, Japan*
[d]*AdSM, Hiroshima University, Higashi-Hiroshima 739-8530, Japan*

Keywords: mineral tetrahedrite, metal - semiconductor transition

Mineral tetrahedrite $Cu_{12}Sb_4S_{13}$ is expected as one of candidates for environmental friendliness thermoelectric materials because of its low electrical resistivity, low thermal conductivity and high thermopower [1]. The thermoelectric dimensionless figure of merit ZT is estimated to be 0.13 at 340 K. The ZT-value increases by Ni-substitution for the Cu ion and $ZT = 0.7$ is achieved at 665 K for $Cu_{10.5}Ni_{1.5}Sb_4S_{13}$ [2]. On the other hand, $Cu_{12}Sb_4S_{13}$ exhibits a metal semiconductor transition (MST) at $T_{MST} = 85$ K [1]. The metallic electrical resistivity above T_{MST} sharply increases by one order of magnitude at T_{MST} and shows a semiconducting behavior below T_{MST}. The mechanism of the MST is under investigation. In this study, we have investigated temperature dependence of the electronic structure of $Cu_{12}Sb_4S_{13}$ around the Fermi level (E_F) by means of synchrotron radiation photoemission spectroscopy (PES). The unoccupied electronic structure has also been investigated by means of inverse-photoemission spectroscopy (IPES). For comparison, we carried out PES and IPES for the Zn-substituted system $Cu_{10}Zn_2Sb_4S_{13}$, which is categorized to be a semiconductor from the resistivity measurements [1]. The PES experiments were performed at BL-7 of Hiroshima Synchrotron Radiation Center (HSRC) and the IPES spectra were measured using the IPES spectrometer working at HSRC. Clean surfaces of the polycrystalline samples were prepared by fracturing *in situ*.

Figure 1 (a) shows the PES spectra in the vicinity of E_F measured at $h\nu = 25$ eV between 150 and 25 K. No noticeable structure is observed and we notice only a weak and broad structure in the range from 0.15 eV to E_F. The PES intensity is substantially low still in the metallic phase ($T = 150$ K). According to the band-structure calculation [3], E_F is located inside the valence bands and the band gap of 1.3 eV exists above only 0.1 eV. The low intensity well reflects this situation. With decreasing temperature, the intensity of the weak and broad structure gradually decreases though the change is relatively small above 90 K. In order to emphasize the temperature dependence of the spectra arising from the MST, we assume the background constructed from the PES spectrum at 25 K as shown by a dashed line in Fig. 1 (a) and subtract the background from each spectra. The results are shown in Fig. 1 (b) and the integrated intensities between -0.05 and 0.10 eV of the subtracted spectra are plotted as a function of temperature in Fig. 1 (c). The intensity gradually decreases on cooling and an amount of the decrease becomes steep around T_{MST}. Thus, the MST is observed as the decrease of density of states (DOS). The decrease is, however, rather continuous in contrast to the sharp change of the resistivity.

Figure 2 (a) shows the PES spectra of $Cu_{12}Sb_4S_{13}$ and $Cu_{10}Zn_2Sb_4S_{13}$ around E_F measured at $h\nu = 40$ eV and $T = 150$ K. No spectral intensity is detected in consistent with the semiconducting behaviour of the electrical resistivity below room temperature [1]. According to the band-structure calculation of $Cu_{12}Sb_4S_{13}$ [3], just two electronic states are unoccupied for the valence bands. Since, in unit of $Cu_{12}Sb_4S_{13}$, one Zn-substitution for one Cu ion gives just one electron into $Cu_{12}Sb_4S_{13}$, the valence bands are just filled for $Cu_{10}Zn_2Sb_4S_{13}$, which qualitatively describe a semiconducting behavior of the electrical resistivity [1]. The energy gap is estimated to be 320 meV from the leading edge of the spectra. Figure 2 (b) shows comparison of the IPES spectra between $Cu_{12}Sb_4S_{13}$ and $Cu_{10}Zn_2Sb_4S_{13}$. The spectra were measured with the incidence electron kinetic energy of $E_K = 50$ eV. A whole spectral feature is similar. We notice that the rise above E_F of $Cu_{10}Zn_2Sb_4S_{13}$ is slightly shifted to higher energy side compared to that of $Cu_{12}Sb_4S_{13}$, suggesting that energy gap is formed in the unoccupied side.

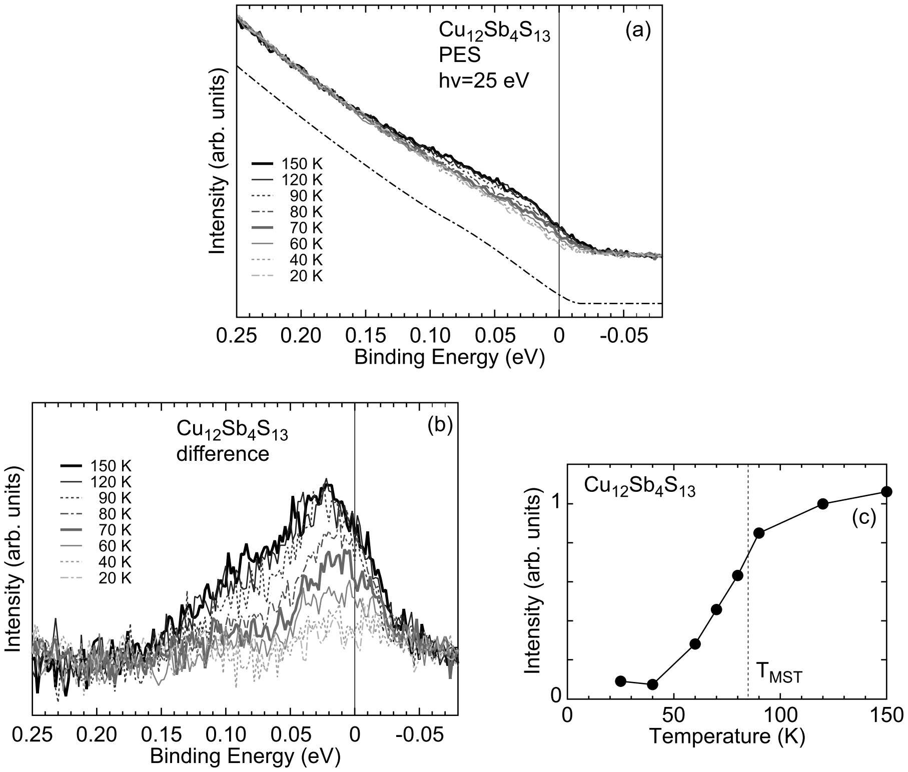

FIGURE 1. (a) Temperature dependence of PES spectra of $Cu_{12}Sb_4S_{13}$ measured at $h\nu = 25$ eV between $T = 150$ and 20 K. Dash-dotted line shows a background constructed by smoothing the spectrum at 20 K. (b) Difference spectra from background (Dash-dotted line in (a)). (c) Integrated intensity of the difference spectra between 0.10 and -0.05 eV in (b).

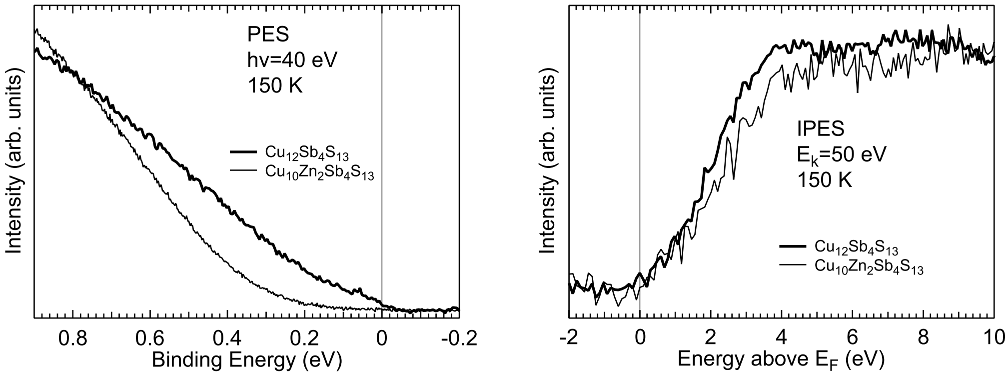

FIGURE 2. (a) PES spectra of $Cu_{12}Sb_4S_{13}$ and $Cu_{10}Zn_2Sb_4S_{13}$ measured at $h\nu = 40$ eV and $T = 150$ K. (b) IPES spectra of $Cu_{12}Sb_4S_{13}$ and $Cu_{10}Zn_2Sb_4S_{13}$ measured at $E_K = 50$ eV and $T = 300$ K.

REFERENCES

1. K. Suekuni *et al.*, Appl. Phys. Exp. **5**, 051201 (2012).
2. K. Suekuni *et al.*, J. Appl. Phys. **113**, 043712 (2013).
3. K. Suekuni *et al.*, J. Appl. Phys. **115**, 143702 (2014).

Validity of the Circular Dichroism in Angle-Resolved Photoemission Spectrum of the High Temperature Superconductor Bi2212

Junfeng He[a], Shang Gao[a], Thomas R. Mion[a], M. Arita[b], K. Shimada[b], G. D. Gu[c] and Rui-hua He[a]

[a] Department of Physics, Boston College, Chestnut Hill, Massachusetts 02467, USA
[b]Hiroshima Synchrotron Radiation Center, Hiroshima University, Hiroshima 739-0046, Japan
[c]Condensed Matter Physics and Materials Science Department, Brookhaven National Laboratory, Upton, New York 11973, USA

Keywords: ARPES, Circular Dichroism, Cuprates

One of the most striking phenomena associated with high temperature superconductivity is the pseudogap state. It is believed that a key to understand the mechanism of superconductivity lies in unraveling of the nature of pseudogap phase. Continuous efforts have been made in both theories and experiments, among which a prominent example is the report of circular dichroism in angle-resolved photoemission spectrum of the high temperature superconductor Bi2212 in the pseudogap state. The observed circular dichroism at M (π,0) point of the Brillouin zone was first interpreted as a direct evidence to show the time-reversal symmetry breaking [1]. This result was later challenged by contradict results from other group [2,3]. Alternative explanations were also proposed, suggesting that the circular dichroic signal may come from the superstructures [2,3] and/or distortions in the Bi-O layer [4].

However, despite the arguments about the origin of the observed circular dichroism from different properties of the sample, the technical validity of the circular dichroism from ARPES measurement itself has never been checked. In another word, before any conclusion about the origin of the possible intrinsic circular dichroism be reached, it is the very first step to establish how accurate the experiment needs to be performed to avoid any artifact dichroic signal which may have the same magnitude as the expected intrinsic ones.

It is well documented and generally agreed that the geometric dichroism vanishes if the propagation vector of the light, the normal to the sample surface and the final state momentum are all in a mirror plane of the sample [1-6]. Therefore, any attempt to look for intrinsic circular dichroism should be performed in the mirror plane to avoid geometric dichroism. However, in all the earlier measurements, only one momentum point M (π,0) was supposed to be in the mirror plane, therefore the aforementioned arguments were essentially based on whether there is dichroic effects on this single momentum point. The solidity of this approach lies in the assumption that the geometric dichroism induced by the inaccuracy in determining the momentum position of the M (π,0) point is significantly smaller than the expected intrinsic circular dichroism. This assumption which had been taken as granted, however, may or may not be true in the real measurements, and definitely needs to be checked experimentally.

To this end, we have performed careful circular dichroism measurements on Bi2212 at Beamline-9A of the Hiroshima Synchrotron Radiation Center. With the special ARPES setup at Beamline-9A, we were able to measure a cut instead of a single point in the mirror plane. The Γ (0,0)-Y (π, π) mirror plane of the sample was selected: First, it is free from superstructures and distortions in the Bi-O layer, that it stays as a mirror plane of the sample even with superstructures and distortions. Second, there should be no circular dichroism along Γ (0,0)-Y (π, π) from the time-reversal symmetry breaking induced by the circulating-current in the pseudogap phase [6]. Therefore, it provides an ideal mirror plane to test the geometric dichroism induced by the inaccuracy in determining the momentum positions.

The experimental results are shown in fig.1. It is clear that when the sample is perfectly aligned and the measured cut is exactly in the Γ (0,0)-Y (π, π) mirror plane (fig.1a), there is no circular dichroism as expected (fig.1b). However, the geometric dichroism starts to emerge with a reasonable magnitude (~5% of the spectrum intensity) when the angle is only 0.3 degrees off (fig.1c). It increases to ~10% of the spectrum intensity when the angle offset reaches only 0.5 degrees (fig.1e). The intrinsic circular dichroism induced by the breaking of time-reversal symmetry is estimated to give rise to an asymmetry of ~10% [6] and the one estimated by considering distortions in the Bi-O layer is ~5% [4]. Therefore, an angle offset of ~0.3 degrees gives a geometric dichroism which is comparable to the expected intrinsic ones from the sample. However, an offset of ~0.3 degrees is too small to be corrected in ARPES measurements neither by the Fermi surface mapping (fig.1a) nor the measured cut itself. Our successful identification of the exact Γ (0,0)-Y (π, π) direction is conditional: We know there is no intrinsic circular dichroism, therefore we moved the angles in a step of 0.1 degrees and found out the accurate direction along which there is no dichroism at all. However, this method is not valid when intrinsic and geometric dichroism may coexist, given the fact that they might either enhance or cancel the magnitude of each other. Our findings have clearly established the accuracy limit (at least <0.3 degrees) of the experiment to avoid the geometric dichroism, which is a prerequisite to discuss the intrinsic circular dichroism from the sample, however has yet to be reached. Therefore, the question about circular dichroism in angle-resolved photoemission spectrum of cuprates is still open. The next generation of ARPES analyzer with a 2D detector incorporated with an accurate 6-axis cryostat might give new insights on the way to promote this research.

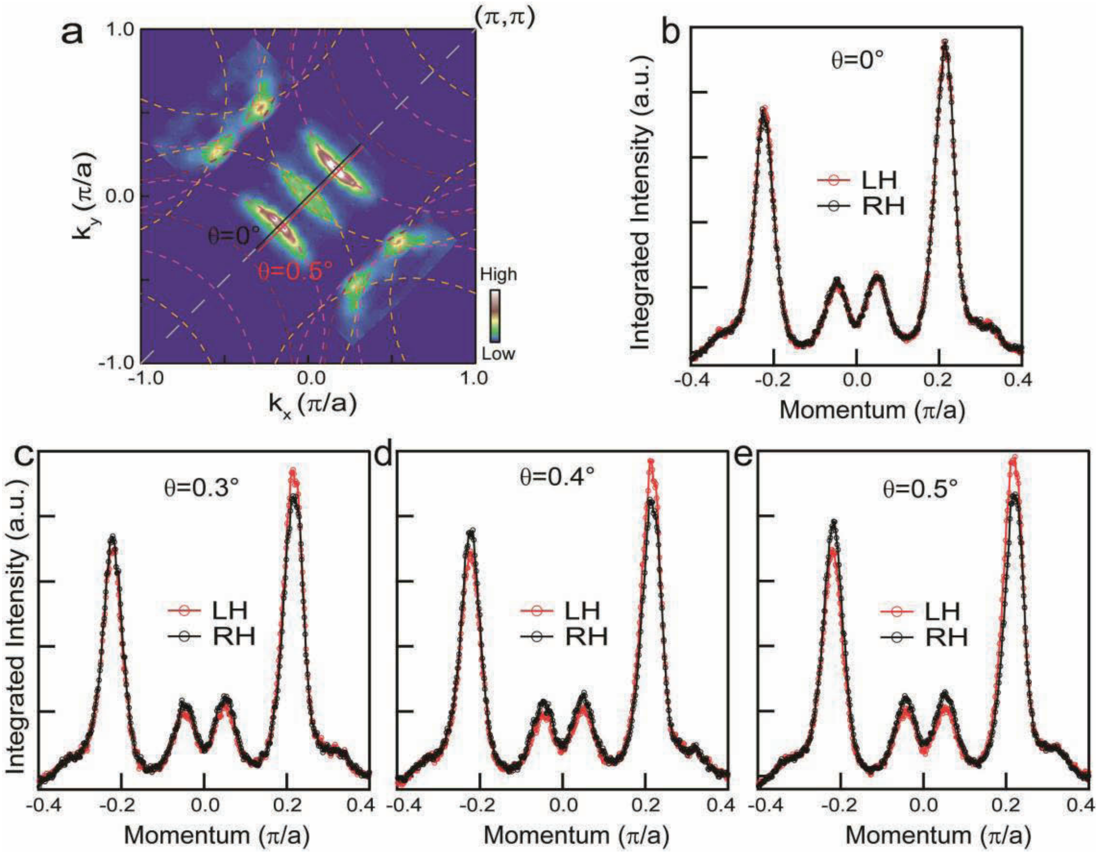

FIGURE 1. Geometric dichroism induced by angle offset. (a), Fermi surface map of an underdoped Bi2212 sample with a superconducting transition temperature of 75K. (b-c), Integrated ARPES intensities probed by left-handed (LH) and right-handed (RH) polarized light along momentum cuts with an angle offset of 0, 0.3, 0.4, 0.5 degrees respectively. All the measurements were done at 30K with a photon energy of 21.2eV.

REFERENCES

1. A. Kaminski et al., *Nature* **416**, 610 (2002).
2. S. V. Borisenko et al., *Phys. Rev. Lett.* **92**, 207001 (2004).
3. S. V. Borisenko et al., *Nature*, doi:10.1038/nature02931 (2004).
4. V. Arpiainen et al., *Phys. Rev. Lett.* **103**, 067005 (2009).
5. J. C. Campuzano et al., *Nature,* doi:10.1038/nature02932 (2004).
6. C. M. Varma, *Phys. Rev. B* ***61,*** R3804-R3807 (2000).

14-A-11　BL-9A

Band structure of $Pr_2Ir_2O_7$ studied by ARPES

T. Kondo[a] , M. Nakayama[a] , W. Malaeb [a], J.J. Ishikawa [a],
S. Nakatsuji [a], and S. Shin [a]

[a] ISSP, University of Tokyo, Kashiwa, Chiba 277-8581, Japan

Keywords: ARPES, Strongly correlated system, Topological quantum phase

Strong spin-orbit coupling fosters exotic electronic states such as topological insulators and superconductors, but the combination of strong spin-orbit and strong electron-electron interactions is just beginning to be understood. Central to this emerging area are the 5*d* transition metal iridium oxides [1,2]. The main goal of the study we propose is to identify, by using ARPES, the new-types of correlated topological states theoretically predicted in pyrochlore iridates, such as topological Mott insulator, Weyl semi-metal, topological Fermi arc, and quantum spin and anomalous Hall states [3,4].

Following the discovery of topological insulators, the next frontier is the regime in which both spin-orbit coupling and correlation effects are strong. Theory has suggested that the pyrochlore iridates ($Ln_2Ir_2O_7$; *Ln*=rare earth elements), a family of cubic 5*d* transition metal oxides, realize both band inversion [2,3], the essential ingredient of topological insulators, and strong correlations. The phenomenological suggestion is that the Fermi surface of $Pr_2Ir_2O_7$ contains a single Fermi node at the Γ point protected by cubic and time-reversal symmetries, which emerges as the touching point of two quadratically dispersing "conduction" and "valence" bands [**Fig.1(a) and Fig.3(b)**]. If the assumption is correct, $Pr_2Ir_2O_7$ could be a strongly correlated analog of HgTe, which has a mathematically identical quadratic node at the Fermi energy and was first recognized as the topological insulator realized in the form of strained thin film. Similarly, the $Pr_2Ir_2O_7$ could be a "parent" state tunable to new-types of strongly correlated topological phases [**Fig.1(b)-(d)**] [2,3]. As the ionic radius of *Ln* site increases (for example, *Ln*=Nd and Eu), the all-in-all-out antiferromagnetic order emerges [inset of **Fig.2(a)**], which causes the time-reversal symmetry breaking in bulk. This could

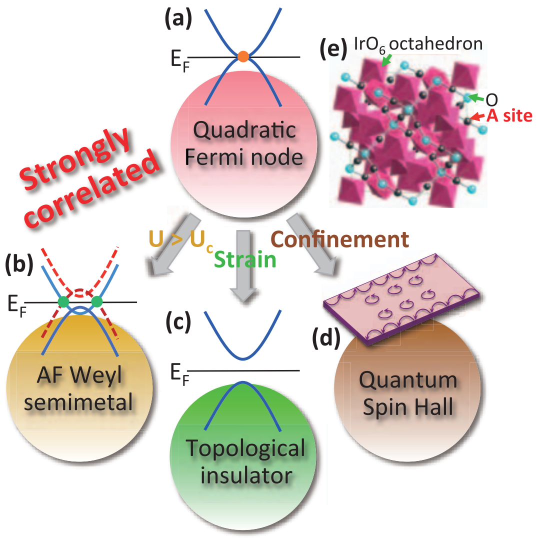

FIGURE 1. Schematic diagram illustrating **(a)** the quadratic Fermi node state of $Pr_2Ir_2O_7$ and its role as a parent of **(b)-(d)** interacting topological phases. **(e)** Crystal structure of pyrochlore iridates ($Ln_2Ir_2O_7$).

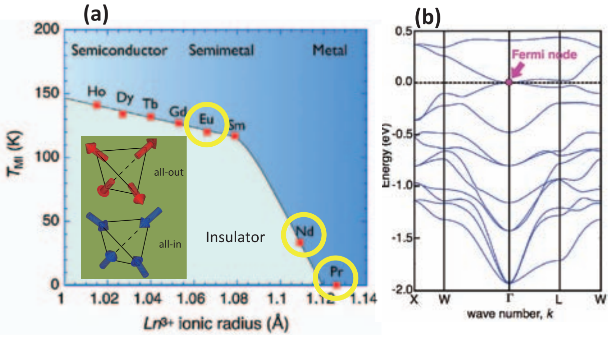

FIGURE 2. **(a)** Phase diagram of pyrochlore iridates ($Ln_2Ir_2O_7$) [5]. **(b)** Our result of band calculation for $Pr_2Ir_2O_7$. Fermi node is marked by a magenta circle. We have grown high quality single crystals of three compounds (marked by yarrow circles).

provide a realization of Weyl fermions that obeys a two-component Dirac equation. It was also predicted to establish remarkable topological properties manifested by surface states in the form of Fermi arcs [5]. The pyrochlore iridates study therefore has enormous potential to open up the next frontier of condensed matter physics.

By ARPES, we have experimentally realized the Fermi node state in $Pr_2Ir_2O_7$. We observed that a parabolic band-dispersion approaches E_F with increasing photon energies (or k_z values), and finally touches it at the Γ point. With a further increase of k_z, the dispersion gets away from E_F again, which signifies that the 3D band structure of $Pr_2Ir_2O_7$ has a single Fermi point. Other scans of different k_z values up to the L point revealed no other states touching or crossing E_F. This satisfies the charge neutrality, and it could be a further evidence for the realization of nodal state. Figure 3 (a) shows the energy distribution curves measured along a momentum cut across the Γ point. The ARPES spectra are cut-off by the Fermi distribution function, which thus prevents us from examining the energy state close to E_F. To remove the Fermi cut-off effect, we symmetrized the original ARPES spectra about E_F as demonstrated in Fig.3(b). It is revealed that the spectral feature with two peaks merges to one peak along the momentum cut, signifying the quadratic band touching at a single k point. In Figs. 3(d) and 3(e), the symmetrized ARPES image and its 2nd derivative are plotted. It is clearly seen that the parabolic band dispersion touches at E_F as theoretically predicted [Fig.3(c)].

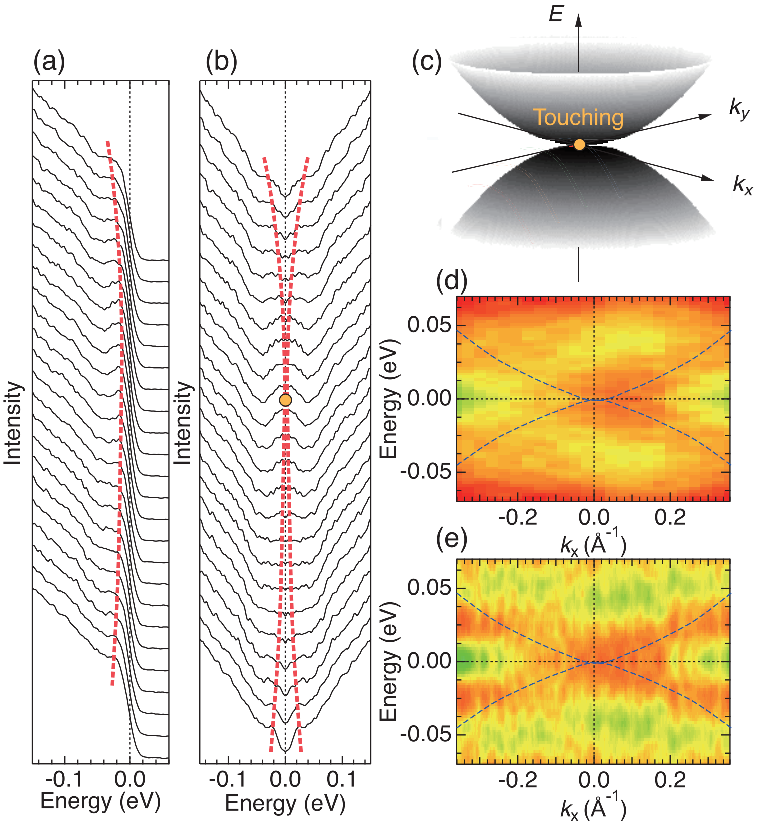

FIGURE 3. (a) Energy distribution curves measured along a momentum cut across the Γ point in $Pr_2Ir_2O_7$. **(b)** The same data as in (b), but symmetrized about the Fermi level; the symmetrization technique is commonly used to remove the Fermi cut-off effect on the ARPES spectra. (c) Schematic picture of the Fermi node state, expected to be realized in $Pr_2Ir_2O_7$. (d) ARPES dispersion map across the Γ point, indicated with a red curve in (c). (e) The same image as in (c), but after the 2nd derivative.

REFERENCES

1. B. Kim *et al.*, *Phys. Rev. Lett.* **101**, 076402 (2008).
2. D. Pesin and L. Balents, *Nat. Phys.* **6**, 376 (2010).
3. E.-G. Moon *et al.*, *Phys. Rev. Lett.* **111**, 206401 (2013).
4. X. Wan *et al.*, *Phys. Rev. B* **83**, 205101 (2011).
5. K. Matsuhira et al., *J. Phys. Soc. Jpn*. **76**, 3706 (2007).

A novel one-dimensional electronic state at $IrTe_2$ surface

T. Mizokawa[a], D. Ootsuki[b], T. Sugimoto[c], M. Takahashi[b], N. L. Saini[d],
M. Horio[e], A. Fujimori[e], S. Pyon[f], K. Kudo[f], M. Nohara[f],
M. Arita[g], H. Anzai[g], H. Namatame[g], M. Taniguchi[g,h]

[a] *Department of Applied Physics, Waseda University, Shinjuku-ku, Tokyo 169-8555, Japan*
[b] *Department of Physics, University of Tokyo, Kashiwa, Chiba 277-8561, Japan*
[c] *Department of Complexity Science and Engineering, University of Tokyo, Kashiwa, Chiba 277-8561, Japan*
[d] *Department of Physics, University of Roma "La Sapienza", Piazzale Aldo Moro 2, 00185 Roma, Italy*
[e] *Department of Physics, University of Tokyo, Bunkyo-ku, Tokyo 113-0033, Japan*
[f] *Department of Physics, Okayama University, Sendai 980-8578, Japan*
[g] *HiSOR, Hiroshima University, Higashihiroshima, Hiroshima 739-0046, Japan*
[h] *Graduate School of Science, Hiroshima University, Higashihiroshima, Hiroshima 739-8526, Japan*

Keywords: orbital physics, surface state, one-dimensional electronic state, Ir chalcogenide

$Ir_{1-x}Pt_xTe_2$ and related systems have been attracting great interest since the Ir/Te triangular lattice layer exhibits superconductivity with maximum $T_c \sim 3.1$ K as reported by Pyon *et al.* [1] and Yang *et al.* [2] The parent material $IrTe_2$ undergoes a structural phase transition at ~ 270 K that should be driven by the Ir 5*d*/Te 5*p* orbital and charge order. The Pt substitution for Ir suppresses the Ir 5*d*/Te 5*p* orbital and charge order, and induces the superconductivity. We have performed angle-resolved photoemission spectroscopy (ARPES) on $IrTe_2$ and $Ir_{0.95}Pt_{0.05}Te_2$ at BL-9A and revealed the unique electronic structure [5,6]. $IrTe_2$ in the undistorted phase and superconducting $Ir_{0.95}Pt_{0.05}Te_2$ have multi-band Fermi surfaces with six-fold symmetry (one outer Fermi surface with flower shape and six inner Fermi pockets) which are basically consistent with band-structure calculations [5,6]. $IrTe_2$ in the structurally distorted phase shows very complicated Fermi surfaces including the straight Fermi surfaces reported in ref. 5. The anisotropic Fermi surfaces indicate that the Ir 5*d*/Te 5*p* orbital symmetry breaking plays important roles in the structural distortion and would be consistent with the orbitally-induced Peierls mechanism [7,8]. However, the straight Fermi surfaces were observed only when the $IrTe_2$ crystals were cleaved at room temperature and then cooled down to the low temperature. In order to clarify the origin of the straight Fermi surfaces observed in $IrTe_2$, we have measured photon energy dependence of ARPES.

Figure 1(a) shows the ARPES results taken at 20 K for $IrTe_2$. The crystals were cleaved at 300 K and then slowly cooled down to 20 K for the measurements. The photon energies were varied from 17 eV to 32 eV. The straight Fermi surfaces reported in ref. 5 were clearly observed. As shown in the Fermi surface map in the k_x-k_z plane (Fig. 1(b), k_x: momentum along the one-dimensional band dispersion, k_z: momentum perpendicular to the surface), they do not change appreciably with the photon energy whereas the other complicated Fermi surfaces strongly depend on it. Therefore, the complicated Fermi surfaces with the strong k_z dependence can be assigned to the bulk of $IrTe_2$ with Ir/Te orbital and charge order. On the other hand, the straight Fermi surfaces should be assigned to the surface of $IrTe_2$. The straight Fermi surfaces are derived from the very one-dimensional band dispersion along the k_x direction. It is highly interesting how such a one-dimensional electronic state can be realized on the triangular lattice layer. A possible fascinating scenario is that the bulk orbital ordered state forms anisotropic domains along the *x* direction and the surface electronic states are created at the one-dimensional and straight boundaries between the domains.

In addition to the main one-dimensional band, several branches are clearly observed well below the Fermi level in Fig. 1(a), suggesting that the electrons are confined along the *y* and *z* directions. Since the velocity of the confined electron V_F is ~ 1 eV· Å and the energy separation between the neighboring branches ΔE is ~ 0.15 eV, the length scale of the confinement would $2\pi V_F / \Delta E \sim 25$ Å. This value is comparable to the lattice constant of the distorted phase would be consistent with the domain boundary scenario. The present result indicates that the surface of $IrTe_2$ and related materials can be a new playground to explore novel one-dimensional electronic states. The one dimensional electronic state is naturally formed due to the orbital and charge ordering in the bulk. In particular, the strong spin-orbit interaction of the Ir 5d and Te 5p subshells can be exploited for realization of new spintronics or orbitronics devices. The effect of the spin-orbit interaction should be studied in future by means of spin-resolved photoemission spectroscopy.

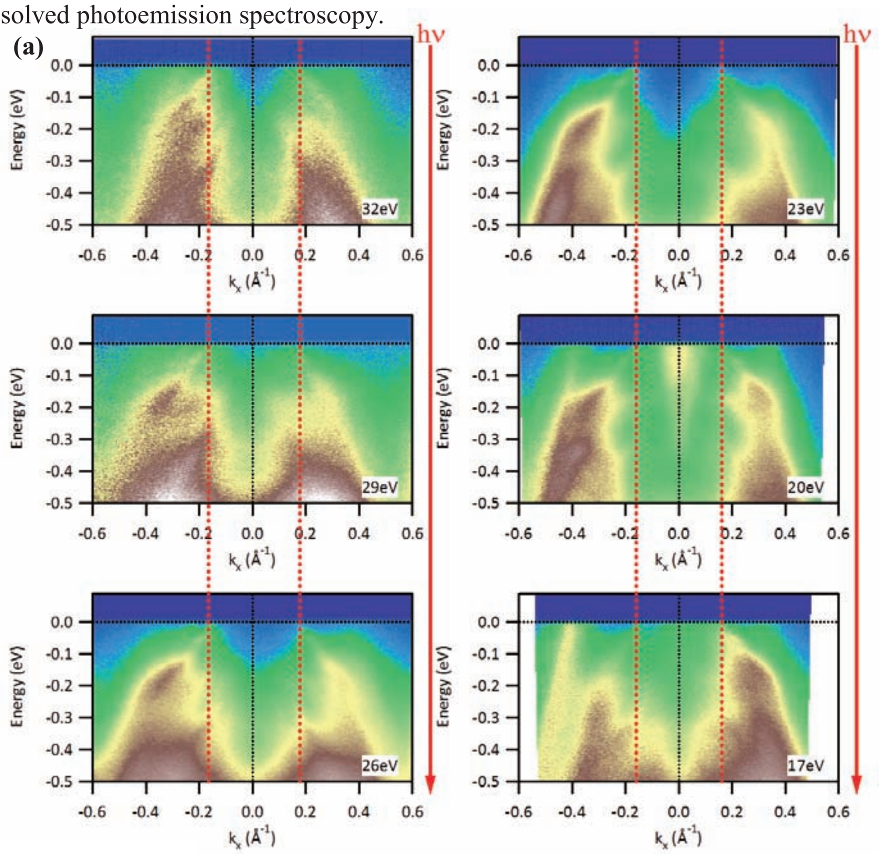

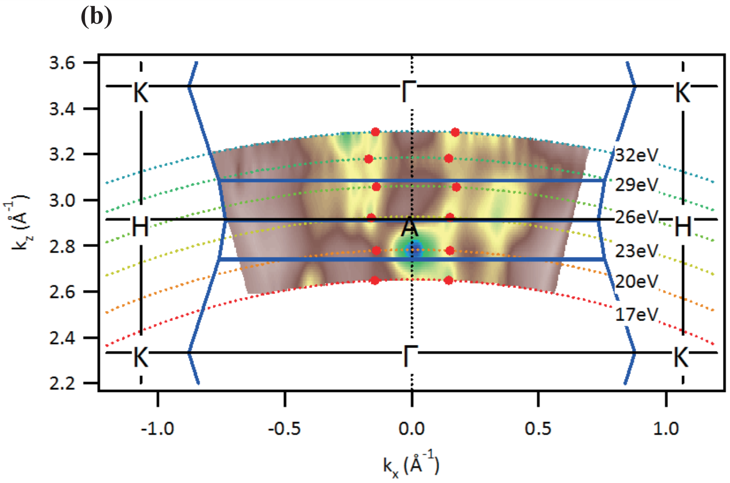

FIGURE 1. (a) ARPES spectra of IrTe$_2$ along the Γ-K or A-H direction (k_x direction) taken at 20 K and hν = 32, 29, 26, 23, 20, and 17 eV. The dotted lines roughly indicate the Fermi wave number at which the surface band crosses the Fermi level.
(b) Fermi surface map in the k_x-k_z plane. k_z is the electron momentum perpendicular to the cleaved surface.

REFERENCES

1. S. Pyon, K. Kudo, and M. Nohara, *J. Phys. Soc. Jpn*. **81**, 053701 (2012).
2. J. J. Yang, Y. J. Choi, Y. S. Oh, A. Hogan, Y. Horibe, K. Kim, B. I. Min, and S-W. Cheong, Phys. Rev. Lett. **108**, 116402 (2012).
3. S. Jobic, R. Brec, and J. Rouxel, J. Solid State Chem. **96**, 169 (1992).
4. N. Matsumoto, K. Taniguchi, R. Endoh, H. Takano, and S. Nagata, J. Low Temp. Phys. **117**, 1129 (1999).
5. D. Ootsuki, S. Pyon, K. Kudo, M. Nohara, M. Horio, T. Yoshida, A. Fujimori, M. Arita, H. Anzai, H. Namatame, M. Taniguchi, N. L. Saini, and T. Mizokawa, *J. Phys. Soc. Jpn*., **82**, 093704 (2013).
6. D. Ootsuki, T. Toriyama, M. Kobayashi, S. Pyon, K. Kudo, M. Nohara, T. Sugimoto, T. Yoshida, M. Horio, A. Fujimori, M. Arita, H. Anzai, H. Namatame, M. Taniguchi, N. L. Saini, T. Konishi, Y. Ohta, and T. Mizokawa, *J. Phys. Soc. Jpn*. **83**, 033704 (2014).
7. D. I. Khomskii and T. Mizokawa, *Phys. Rev. Lett*. **94**, 156402 (2005).
8. D. Ootsuki, Y. Wakisaka, S. Pyon, K. Kudo, M. Nohara, M. Arita, H. Anzai, H. Namatame, M. Taniguchi, N. L. Saini, and T. Mizokawa, *Phys. Rev. B* **86**, 014519 (2012).

Temperature Dependence of Fermi Surface in Mixed-Valent EuPtP

H. Anzai[a], K. Ichiki[a], M. Arita[b], H. Namatame[b], M. Taniguchi[b,c],
M. Mitsuda[d], M. Umeda[d], H. Wada[d], H. Ikeda[e], and K. Mimura[a,b]

[a] *Graduate School of Engineering, Osaka Prefecture University, Sakai 599-8531, Japan*
[b] *Hiroshima Synchrotron Radiation Center, Hiroshima University, Higashi-Hiroshima 739-0046, Japan*
[c] *Graduate School of Science, Hiroshima University, Higashi-Hiroshima 739-8526, Japan*
[d] *Department of Physics, Graduate School of Science, Kyushu University, Fukuoka 812-8581, Japan*
[e] *Department of Physics, Ritsumeikan University, Kusatsu Shiga 525-8577, Japan*

Keywords: *f*-electron, Electronic structure, Angle-resolved photoemission spectroscopy.

The ternary rare-earth compound EuPtP shows two first-order valence transitions at T_1 = 235 K and T_2 = 190 K [1,2,3], and the mean Eu valence changes from a magnetic divalent $4f^7$ state to a non-magnetic trivalent $4f^6$ state with decreasing temperature. These two valence transitions cause an anomalous enhancement of the *c*-axis resistivity between two valence transitions ($T_2 < T < T_1$), and the resistivity approaches the limit of metallic conduction. In general, the conductivity of a free electron meal at low temperature is proportional to the density of conduction electrons near Fermi energy (E_F) [4]. Therefore, a comprehensive understanding of topology of Fermi surface (FS) and its volume would provide important insight into the origin of the mechanism for the valence transition in EuPtP.

Angle-resolved photoemission spectroscopy (ARPES) has played a leading role in the investigating the electric state near E_F. However, the study of the valence transition has been hindered, because only a few Eu-based compounds have good cleavage plane, which is required for the ARPES measurement. While a recent ARPES study for mixed-valent $EuNi_2P_2$ has revealed that the Ni 3*d* bands indeed cross the E_F, the FS topology has still been unclear [5].

Here, we report the high-resolution ARPES study of temperature dependence of the FS in EuPtP for the first time. The ARPES measurements were performed at BL-9A of Hiroshima Synchrotron Radiation Center, where the two different linear polarizations (*s*- and *p*-polarized light) were achieved from APPLE II type undulator. Total instrumental energy and momentum resolutions were set at 10 meV and 0.008 $Å^{-1}$, respectively. The samples were cleaved *in situ* and kept under ultrahigh vacuum better than 5 x 10^{-11} Torr.

Figures 1(a) and 1(b) show the ARPES spectra measured at T = 260 K (above T_1) along the Γ-M direction (cut #1) and off the direction (cut #2), respectively. The Eu $4f^6$ multiplets are observed as a featureless continuum in the region from -0.5 to -1.0 eV due to finite resolution effects. Near E_F, three dispersive hole-like bands, α, β, and γ, can be identified. They mainly originate from Pt 5*d* orbitals and overlap the multiplet terms. As shown by energy distribution curves (EDCs) in Fig. 1(d) near K point, the β and γ bands clearly cross E_F. Therefore, there are two hole-type FSs around K point, and one hole-type FS around Γ point, as shown in Fig. 1(c). The α FS is nearly circular with enclosed area of ~ 11% of the Brillouin zone area. The β and γ FSs are triangle-like shape with an area of ~ 4% and ~ 23%, respectively.

By comparing the electric structure above and below T_1, downward band shifts could be identified for the β and the γ bands. As shown in Fig. 1(g), the β and the γ bands moves away from E_F, and the top of the γ band is at about -0.2 eV below E_F. There are now one hole-like α FS around Γ point and one triangle-like β FS. The estimated area of the α and the β FSs with respect to the Brillouin zone is ~11% and ~18%, respectively. The shrinking FS implies that the Pt 5*d* electron is disappearing from the Fermi volume, and as a result, electrical resistivity may increase between the two-valence transitions.

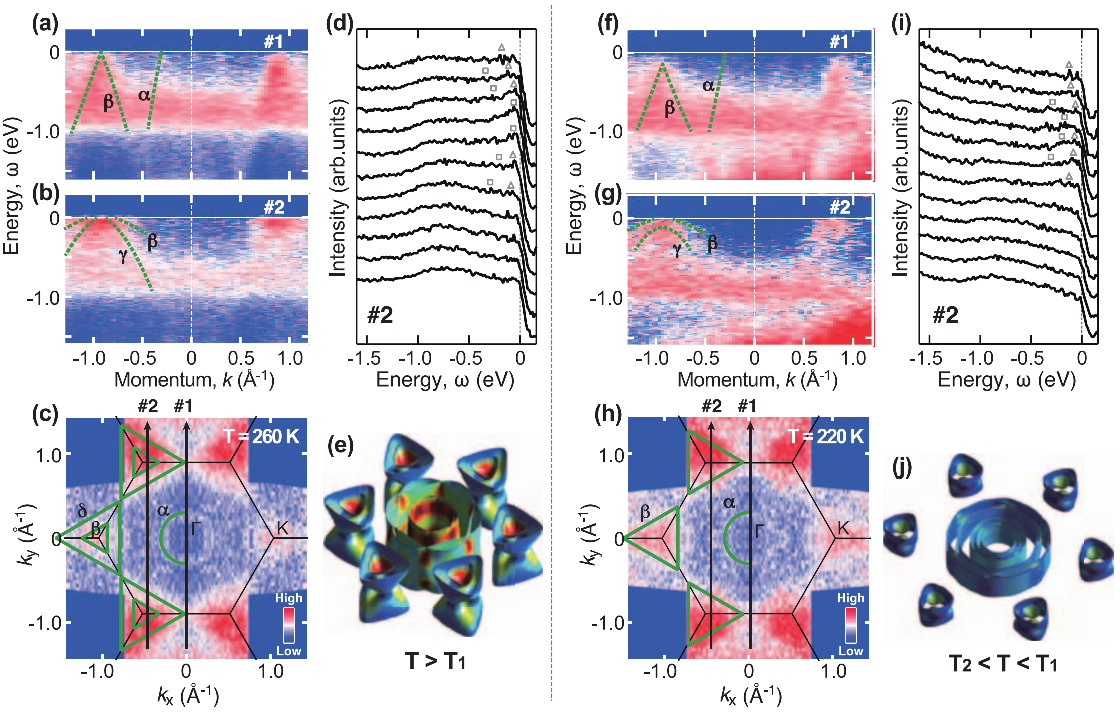

Figure 1 Electric structure of EuPtP taken with *s* polarization and photon energy of $h\nu = 34$ eV. (**a**)(**b**) ARPES intensity plots as indicated the black arrows in panel (c). Green dashed lines in (a) and (b) are guide to the eye. (**c**) Fermi surface mapping in the Brillouin zone integrated over $0 < |\omega| < 300$ meV. (**d**) Energy distribution curves around *K* point for the data in panel (b). Data were taken at $T = 260$ K (above T_1). (**f**), (**g**), (**h**), and (**i**) are the same as in panel (a), (b), (c), (d) and (e), respectively, but taken at $T = 220$ K ($T_2 < T < T_1$). (**e**)(**j**) The calculated Fermi surface above T_1 and within $T_2 < T < T_1$, respectively.

In Figs. 1(e) and 1(j), we show FSs predicted by the first-principle calculation. At first glance, the bands do not show much k_z dispersion, because the EuPtP is quasi-two dimensional system. Around the *K* point, the shrinking FS with the valence transition is roughly reproduced by the calculations. However, one finds that the number and topology of the calculated FSs around Γ point is different from that of the measured one. We note that in order to obtain accurate FS topology, it is crucial to compare the data taken with *p*- and *s*-polarized light following the dipole selection rule.

In summary, we have revealed the temperature dependence of the FS in EuPtP from the high-resolution ARPES for the first time. The experimentally determined FS above T_1 consists of three types of hole pockets, one centered at the Γ point, two around the *K* point. The area of FS shrinks due to the downward energy shift of the bands, resulting in the reduction of the Fermi volume which is likely responsible for the anomalous enhancement of *c*-axis resistivity.

References

[1] N. Lossau *et al.*, Z. Phys. B **74**, 227 (1989).
[2] N. Lossau *et al.*, Z. Phys. B **77**, 393 (1989).
[3] G. Michels *et al.*, Z. Phys. B **98**, 75 (1995).
[4] C. Kittel, *Solid State Physics* (John Wiley & Sons, New York, 1996).
[5] S. Danzenbächer *et al.*, Phys. Rev. Lett. **102**, 026403 (2009).